Structural and Geologic Mapping of Northern Tellus Regio, Venus: Implications for Crustal Plateau Evolution

A Thesis

SUBMITTED TO THE FACULTY OF

UNIVERSITY OF MINNESOTA

BY

Aaron Slonecker

IN PARTIAL FULFILLMENT OF THE REQUIREMENTS

FOR THE DEGREE OF

MASTER OF SCIENCE

Vicki Hansen

December 2013

ACKNOWLEDGEMENTS

I would like to thank my advisor, Dr. Vicki Hansen, for the continued guidance and support over the past two years. The positive feedback provided to me throughout my research and writing obstacles, helped me to become a better and more complete scientist and individual. I would also like to thank my committee members, Dr. John Goodge and Kate Carlson, for their patience and encouraging remarks throughout my time at UMD. Last, but not least I would like to thank my friends and fellow graduate students for continued positive support and for being a part of memories I will cherish and never forget.

To my family and friends
for their constant love and support

Abstract

Crustal plateaus, one type of large surface feature on Venus, are features that no longer form today, and represent ancient geodynamic processes. Crustal plateaus host distinctive tectonic fabric, referred to as ribbon tesserae terrain. The formation of crustal plateaus is a highly debated topic with the major differences in surface deformation and plateau support. Each hypothesis also has different mechanisms that form the crustal plateau, which leads to slightly different spatial and temporal relationships between structures. Detailed mapping of northern Tellus Regio displays deformational structures across the study area and provides clues for crustal plateau evolution. The study area, divided into domains based on topography and surface roughness, displays structures occurring in specific domains and structures occurring within multiple domains. Spatial and temporal relationships of structures between domains provide insight into crustal plateau evolution and the deformational interactions between crustal plateaus and lowlands. Structural relationships in northern Tellus Regio indicate that short-wavelength structures form early on, and wavelengths of structures increase with time. The mapping of this study displays structural trends and temporal relationships, and provides a way of identifying and defining the northern boundary of Tellus Regio. Geologic mapping shows that Tellus Regio extends north up to 60°N and contains a large area of highly deformed deposited material. The collision between this northern part of Tellus Regio and a separate crustal plateau led to a folded terrain and raises questions regarding the evolution of individual crustal plateaus, as well as interactions of multiple crustal plateaus.

TABLE OF CONTENTS

LIST OF ILLUSTRATIONS

Supplementary Files

1. INTRODUCTION

Venus, our sister planet, is similar in size, density, distance from the sun, and composition to Earth, and yet does not have plate tectonics, the process by which Earth cools. Because Venus is so similar to the Earth and yet does not have plate tectonics the question of how Venus cools arises. Surface features on a planet form as a result of planetary cooling, so by understanding how surface features form and the history of their formation on Venus, we gather clues to understand the cooling mechanism.

More than 80% of the surface of Venus is composed of crustal plateaus, volcanic rises, and volcanic plains, herein referred to as lowlands (Phillips and Hansen 1998). Crustal plateaus and volcanic rises are higher in elevation than the volcanic plains, but cover a smaller area of Venus. Crustal plateaus and volcanic rises are similar in size and general shape, however their differences include interpreted ages and surface features. Volcanic rises are young, contemporary features interpreted to be surface expressions of mantle plumes. Crustal plateaus on the other hand represent ancient features and record ancient geodynamic processes, although the nature of those processes are unknown. Volcanic rises are characterized by flows and show widespread evidence of volcanic processes whereas, crustal plateaus are characterized by ribbon tesserae terrain (RTT), a structural fabric that characterizes all crustal plateaus but also occurs as inliers in lowlands. RTT is characterized by high relief relative to the surroundings, high surface roughness, intersecting sets of tectonic lineaments (Basilevsky et al. 1986) and intratessera basins (ITBs) (Banks and Hansen 2000). The topographic and structural boundaries of crustal plateaus are commonly the same.

Crustal plateaus mark the oldest large surface features on Venus, and provide insight into early crustal processes. The formation of crustal plateaus is a highly debated subject. The four major hypotheses for crustal plateau formation are mantle downwelling (Bindschadler and Head 1991), mantle upwelling (Hansen et al. 1997), pulsating continents (Romeo and Turcotte 2008), and lava-pond and bolide impact (Hansen 2006). All of these hypotheses agree that crustal plateaus formed with a thin global lithosphere, but the mechanism responsible for plateau deformation and uplift is different. All four formation hypotheses need to address the overall shape and height of crustal plateaus, and the spatial and temporal relationships between structures observed.

Tellus Regio is a crustal plateau centered at 42.6°N/76.8°E (Fig. 1). It is one of two isolated crustal plateaus and is a prime candidate for further studies of crustal plateau evolution. Tellus Regio is heart-shaped with sharp and distinct western, southern, and eastern topographic boundaries with the surrounding lowlands. Previous studies have focused on the southern part of Tellus Regio, leaving the northern area mostly forgotten. Northern Tellus Regio includes areas of both RTT and lowlands, however the northern boundary of Tellus Regio is poorly defined, and could aid in understanding the evolution of crustal plateaus and their interactions with lowlands.

This study focuses on northern Tellus Regio, with the specific goal of defining the northern boundary. Defining the northern boundary and determining the history of northern Tellus Regio can provide further insight into crustal plateau evolution and a better understanding of Venus's ancient processes. The spatial and temporal relationships between structures allow for examination and evaluation of crustal plateau hypotheses.

2. BACKGROUND

2.1 Surface features on Venus

Venus has a mean planetary radius of 6051.84 km (MPR) (Ford and Pettengill 1992). The surface is made of highlands, mesolands, and lowlands. There are four types of large surface features, Ishtar Terra, Artemis, volcanic rises and crustal plateaus (Fig. 1). Ishtar Terra and Artemis are both unique features on Venus and will not be discussed in this paper. Both volcanic rises and crustal plateaus are circular to quasi-circular in planform with similar diameters ~1,000 – 2,500 km, and rise ~0.5 – 4 km above the surrounding terrain; however volcanic rises and crustal plateaus differ in topographic shape, isostatic support, interpreted ages, and surface features (Phillips and Hansen 1994). Volcanic rises are dome-like with broad topographic rises, compared to crustal plateaus that are flat-topped with steep sides. Gravity-topography ratios indicate that volcanic rises have deep apparent depths of compensation, taken as thermal support, whereas crustal plateaus have shallow apparent depths of compensation interpreted as supported by either thick crust or low-density material in the upper mantle. Volcanic rises are widely interpreted as surface expressions of mantle upwellings and are young, contemporary features (Phillips and Hansen 1994, Bindschadler et al. 1992), whereas crustal plateaus are considered to be ancient surface features. The surfaces of volcanic rises are composed of volcanic flows, exhibiting widespread volcanism, compared to crustal plateaus, which have surfaces characterized by ribbon tesserae terrain (RTT).

RTT makes up 12% of the surface of Venus (Hansen and Lopez 2010) and occurs as large tracts mostly in crustal plateaus, but also occurs as scattered inliers of RTT across both mesolands and lowlands. RTT is characterized by high relief relative to the

surroundings, high surface roughness, intersecting sets of tectonic lineaments (Basilevsky et al. 1986), and intratessera basins (ITBs) (Banks and Hansen 2000). Tectonic lineaments consist of folds, graben complexes, and ribbon structures. Short-, medium-, and long-λ folds represent contractional structures, typically marked by gradational slopes between crests and troughs in radar images. Graben complexes and ribbon structures are both extensional structures, but differ in size and shape. Graben complexes have smaller length-width aspect ratios, and inward dipping slopes are interpreted as ~60°. Ribbon structures, with larger length-width aspect ratios are defined by periodic alternating flat-topped ridges and flat-bottomed troughs connected by steep walls (Hansen and Willis 1998).

Lowlands or volcanic plains comprise over 80% of the surface of Venus (Head et al. 1992). Lowland plains range in elevation between ~1.5 km below MPR to 2 km above MPR, and primarily show regions of low backscatter, radar-dark material, interpreted to consist of both, large sheets of lava flows and volcanic constructs. Lava sheets are indicative of flood volcanism consisting of high effusion rates of low viscosity lava similar to basalt (Guest et al. 1992). Volcanic plains display a variety of large-scale (coronae, ovoids and arachnoids) and smaller-scale (shields) volcanic features (Head et al. 1992).

Crustal plateaus are large, ancient features on Venus that give us insight into processes that were at work in the past. Understanding those processes and how crustal plateaus have evolved provides a way of understanding the past surface of Venus. The combination of understanding ancient processes and current processes will lead to a more complete understanding of the history of Venus.

2.2 Formation Hypotheses of Crustal Plateaus

There are four hypotheses for crustal plateau formation: mantle downwelling (Bindschadler et al. 1992), mantle upwelling (Phillips and Hansen 1998), pulsating continents (Romeo and Turcotte 2008), and lava-pond and bolide impact (Hansen 2000). All four hypotheses include an initial thin global lithosphere, however each differ in the timing of structures formed and the processes responsible for crustal plateau formation. These four hypotheses predict different evolutions of crustal plateaus, but all hypotheses need to address these observations: the presence of RTT and ITBs, the steep-sided, flat-topped overall shape, the type of isostatic support, and why crustal plateaus are not forming today.

In the mantle downwelling hypothesis elevated regions form due to crustal thickening by lower crustal flow accretion, driven by a mantle downwelling (coldspot). Initially crustal material is pulled towards a region of downflow. The downward deflection of the surface forms a circular lowland, resulting in concentrically forming contractional surface feature, while the ductile lower crust pools above the downflow. Through continued downwelling the crust thickens leading to a rise of the highland. Once mantle downwelling ceases, the center of the highland spreads under its own weight creating extensional features and causing the structures in the highland to decrease in elevation, however a highland plateau remains, due to a thickened crust, resulting in isostatic support.

The mantle upwelling hypothesis calls for a mantle plume and resultant partial melting in the upper mantle. The hot mantle plume causes mechanical annealing of the crust, destroying any previous structural anisotropy. The crust heats up, from injection of

magma, and uplifts causing extensional ribbon structures to form. The crust thickens due to magmatic underplating at depth, resulting in the rise of the highland plateau. As the area cools local shortening occurs and the plateau topography flattens because it is unstable. The elevated plateau remains due to the thickened crust. In this hypothesis folds broadly postdate extensional structures.

The pulsating continents hypothesis calls for thick crust due to concentric, thrusting and folding. Similar to the mantle downwelling hypothesis, initially an area of low-density crust is compressed horizontally due to a density driven inversion. This causes shortening of the surface, which is accommodated by concentric thrusting and folding in the margins of the plateau. As the crust thickens, the cold lithospheric mantle develops a gravitational instability under the center of the plateau-continent, and thrust fault and fold interference patterns in the center, begin to form. New lithosphere, generated by heat conduction around the plateau, changes the force balance, and causes the formation of radial graben accompanied by intratessera volcanism. In this hypothesis, within a single cycle, folds generally predate extensional structures, although locally there may be some overlap; volcanic flooding is late. Pulsating continents refers to the proposal that the entire process repeats, progressively accreting more material to the edges of a plateau.

The lava-pond and bolide hypothesis calls for crustal plateau formation due to an external catalyst; impacting the surface with a bolide. This creates massive partial melting in the upper mantle, which makes its way to the surface and creates a huge lava pond. As a result of convection in the lava pond, short-λ folds and orthogonal short-λ ribbon structures form within the solidifying pond "scum". Wavelengths of structures

progressively increase with time due to thickening of the surface layer by progressive cooling and deformation. This process creates the RTT fabric (multiple wavelength structures). Melt within the pond periodically leaks to the surface filling local structural lows, with the last formed lows forming the largest ITBs. The mantle, from which partial melt was derived, forms a depleted solid residuum, which is more buoyant than the surrounding mantle. The low-density mantle melt residuum causes the surface and now solid lava-pond to rise, forming an elevated plateau. This residuum root lies in the ductile mantle and can be stripped away by mantle convection. If the root is stripped away partially or completely the crustal plateau will subside. If however, cooling and thickening of the lithosphere occurred before the root was stripped away, then the crustal plateau would be frozen in place and preserved at the surface. In this hypothesis the formation of folds and ribbon structures broadly overlap in time, with progressively longer-λ structures forming later during pond solidification; local flooding occurs throughout the lava-pond solidification process with the formation of progressive larger ITBs with time.

2.3 Tellus Regio

Tellus Regio, also called Tellus Tessera, is one of two isolated crustal plateaus, and lies centered at 42.6°N/76.8°E in the V10 quadrangle (Fig. 1). Tellus Regio is heart shaped with a slightly longer N-S length (2300 km) than E-W length (1500km), and rises 1-3 km above the surrounding lowlands (Senske and Plaut 2009). The eastern, southern, and western margins are well defined with a sharp boundary between the plateau and the lowlands. The northern boundary and northern extent of Tellus Regio are poorly defined.

The northern part of Tellus Regio includes areas of arcuate lowlands (Leda Planitia) and arcuate suites of RTT inliers (Meni and Dekla Tessera).

2.4 Study Area

The questions of how far north Tellus Regio extends and the nature of Tellus' northern boundary, remain unsolved. Addressing these questions could aid in the understanding of crustal plateau evolution, and is the goal of this research. The study area for this research covers an area over 5×10^6 km^2, from 48°N to 72°N and 55°E to 90°E (Fig. 1). The study area covers the northern half of Meni Tessera, and farther to the north includes Leda Planitia, Dekla Tessera, Audra Planitia, and Fortuna Tessera. Fortuna Tessera makes up the southeastern most area of Ishtar Terra, which continues farther to the north and west, extending 4,000 km (Kaula, et al. 1992). Laima Tessera bounds the western part of the study area. This study area includes highlands, mesolands and lowlands and represents a key place on Venus for not only addressing the extent of northern Tellus Regio, but also examining the structural transition from highlands to lowlands.

2.5 Previous Studies

Previous studies of Tellus Regio focused mostly on the southern area and on individual patches of RTT and ITBs. Other studies have included Tellus Regio in an overall description of crustal plateaus and volcanic rises. Most of the previous studies have excluded the northern boundary, even though this part of Tellus Regio provides an excellent study area for understanding crustal plateau margins.

Bindschadler et al. (1992) analyzed crustal plateaus, including Tellus Regio. In this study, morphologies of structures in Tellus Regio were found to be more complex

than for structures in other crustal plateaus including Ovda and Thetis Regiones. The northern and southern boundaries of Tellus Regio are heavily embayed and there are numerous outliers of complex ridged terrain in the north. This complex ridged terrain is now known as RTT. In the northeast area there is an arc-shaped region with complex RTT.

Detailed geologic mapping focused on ITBs in the south and east parts of Tellus Regio show cross-cutting relationships between ribbon structures, folds, and surface flooding, that indicated that volcanism played a role in the formation of ITBs, during crustal plateau formation (Banks 2000, Banks and Hansen 2000).

Numerous studies of local areas of Tellus Regio (Straley and Gilmore 2007, Gilmore et al. 2009, 2010, 2011, Senske 1999) focused on mapping different tectonic structures and RTT domains, however these works are only published as abstracts. Straley and Gilmore (2007) studied tesserae units with distinct structural features in southwest Tellus and proposed that Tellus Regio was assembled from at least three regions of tesserae, each with distinct tectonic histories. Gilmore and coworkers (2009, 2010, 2011) examined southwest Tellus Regio, dividing the region into different tectonic domains: indenter, fold belt, plateau interior, and a SE geomorphologic unit. Senske (1999), in trying to explain tesserae terrain formation, evaluated relationships between tesserae and adjacent plains. Senske (1999) shows that in many locations "plains lineaments" crosscut both plains and adjacent tesserae indicating that tesserae formation continued after plains emplacement.

The above studies all examined areas within Tellus Regio, but not as a whole. Graupner (2012) examined Tellus Regio from 26N to 42N and provided the first geologic

map of the entire southern area. From mapping and analyzing the spatial and temporal relationships between structures Graupner made three important conclusions: 1) layer thickness increases over time due to the geothermal gradient decreasing, 2) deformation and flooding is synchronous during plateau formation, 3) the 2-D bulk surface strain changed over time.

Previous studies on lowlands are important even if not located within the study area because in the study area both lowlands and crustal plateaus are present. Head et al. (1992) classified volcanic features and structures, some of which include shields, domes, calderas, coronae, and arachnoids. Guest et al. (1992) concluded that a range of different styles of eruptions occurred over time, based on the variety of volcanic forms. McKenzie et al. (1992), saw similarities between pancake-like domes on Venus and simple fluid dynamical models of viscous fluid spreading over a rigid surface.

Sedna Planitia, located around 40N and 345E, contains over 30 arachnoids. Stofan and Head (1986) characterize arachnoids by central volcanic structures surrounded by rings and linear features interpreted to be tectonic. Because arachnoids are formed by both tectonics and volcanism, they are considered magmatotectonic features on Venus. DeShon et al (2000) examined southern Rusalka Planitia, and through geologic mapping showed interactions between topography and structures. The workers found that volcanic plains formation does not occur as discrete episodes of volcanism and deformation, rather a continuous combination of the two.

Few studies to date have focused analysis on the margins of crustal plateaus, yet an understanding of crustal plateau margin histories and processes could provide important constraints for crustal plateau formation. Each of the four plateau formation

hypotheses makes different predictions about margin history. In the mantle downwelling hypothesis, a broad topographic shape forms; in order to get the observed plateau shape there needs to be late faulting at the margins. In the mantle upwelling hypothesis sharp boundaries could occur at the margins, although the margins could be more complex. In the pulsating continents hypothesis, crustal plateaus are pieces of continental crust stacked up by thrust faults and should show a general younging away from the center and towards the margin. In the lava-pond and bolide hypothesis partial collapse of a plateau, from part of the root getting stripped away, would leave behind an area with decreased elevation but containing inliers of RTT.

3. METHODS

3.1 Data

The NASA Magellan mission launched in 1989 and began mapping the surface of Venus in 1990, collecting four global data sets: altimetry, synthetic aperture radar (SAR), gravity, and radiometry (Ford 1993). By the end of the roughly three year mission, Magellan mapped ~98% of the surface revealing information on the planet never before seen. This research utilized the altimetry and SAR data sets to create detailed geologic maps of the surface, and to provide new understanding of structural relationships and evolution between crustal plateaus and lowlands. Gravity and radiometry data is beyond the scope of this project and will not be discussed further.

The altimetry and SAR data sets can be used together for detailed geologic mapping allowing for identification and comparison between structures and topography. The altimeter sensor measured the distance between the spacecraft and the surface with

resolution 10-30 km horizontal resolution. Two types of altimetry data exist, the Altimetry-Radiometry Composite Data Record (ARCDR) and the Global Data Record (GxDR) (Plaut 1993). ARCDR data provides all derived parameters, including radius, rms slope, and reflectivity, in a large table. From this table the GxDR data set was created, and is displayed in map form. The resolution of altimetry data is coarse but illustrates general relationships and transitions between high standing crustal plateaus and adjacent lowlands.

SAR data provides grayscale images of the surface, consisting of both lineaments and areas. Surface topography and roughness can be determined from SAR images. SAR operates at a wavelength of 12.6 cm, the S-band (Ford 1993). The Magellan sensor sends a pulsed microwave signal down to the surface, penetrating Venus's thick, mostly carbon dioxide, atmosphere. The signal scatters when reaching the surface, causing some of the signal to head back to the sensor, depending on slope angle and surface roughness. The incoming signal hits the surface of Venus creating an angle with respect to vertical called the incidence angle. The curvature or the slope of the surface can affect the incidence angle (Farr 1993). If a slope is perpendicular to the path of the signal and hence the incidence angle is zero, almost all of the signal will reflect back and return to the receiver. With increasing surface roughness, more of the signal is scattered back to the antenna. The higher amount of signal scattered back to the receiver the brighter, or whiter, that area appears on the image. If the signal hits a smooth area, it reflects away from the antenna, creating a dark area on the image. SAR resolution is about 100 meters per pixel, allowing for detailed geologic mapping of the surface.

The SAR data set consists of images obtained during three global mapping cycles. Cycle 1 and 3 are both left look, with incidence angles of 35 and 20, respectively: cycle 2 is right look with an incidence angle of 25 (Plaut 1993). The look direction (left look and right look) describes the direction the signal is coming from. Many areas of the planet are covered by more than one cycle, however the northern part of Tellus Regio and the extent of the study area is covered only by cycle 1 data. By combining SAR and altimetry data, synthetic stereo images can be produced, and prove to be useful in geologic mapping (Kirk et al. 1992). Synthetic stereo images, created using a macro developed by Duncan A. Young, were used in this research. The resolution of synthetic stereo is coarse, but the images aid in mapping long-λ structures, which can be difficult to observe otherwise. SAR data provides high-resolution images and allows for detailed mapping of short-λ structures, whereas synthetic stereo images are more useful in identifying long-λ structures.

SAR images are naturally distorted because the sensor is side looking (Farr 1993). There are three main geometric distortions in radar images: foreshortening and elongation, radar layover, and radar shadowing. Foreshortening compresses the image of a mountain's near-range slope and extends or elongates the image of its back slope, thus slope data is not lost, but it is altered. Radar layover is an extreme case of foreshortening, where the top of the mountain is imaged spatially in front of the bottom of the near-range slope, thus the foreground shape data is lost. Radar shadowing is where image data is lost if the slope is steep enough to put the slope in radar shadow. Figure 2 illustrates foreshortening-elongation and radar shadowing. Foreshortening occurs for the slope facing the satellite, whereas elongation occurs at the slope facing away from the satellite.

Radar shadowing also occurs at the slope facing away from the satellite. Radar distortions can be useful in identifying and interpreting geomorphic structures (i.e. radar layover aids in identifying short-wavelength folds).

3.2 Analysis tools

There were four main software packages and mapping tools used during this research: ESRI ArcMap™, MS Excel™, Adobe Photoshop™, and Adobe Illustrator™. Analysis of altimetry data, completed in ArcMap™ provided tables of data that could be exported to Excel™ for the creation of topographic profiles. SAR data, stretched in Photoshop™, provided images that aided in geologic mapping. All geologic and structural mapping was completed in Illustrator™.

Altimetry data in ArcMap™ displays topographic changes across the study area. Excel™ provided easy creation and analysis of topographic profiles to aid in identifying similarities and differences between transects.

Photoshop™ provides a way of stretching SAR images and inverting left-look images. Stretching and inverting SAR images can enhance certain lineaments, allowing for easier recognition and mapping of those lineaments. For example ribbon structures are easier to distinguish in inverted SAR images over regular SAR images. Utilizing both SAR and inverted SAR provides a comprehensive geologic and structural map of the study area. Geologic and structural mapping utilized cycle-1 SAR data, inverted SAR images, and synthetic stereo images.

3.3 Interpretation

Surface features and structures can be interpreted and mapped using SAR. Identifying and interpreting surface structures helps in determining a geologic history of

an area. Mapping structures show crosscutting relationships and relative timing ages. By using both SAR and altimetry data, as well as synthetic stereo, geologic maps can be created to derive surface history and processes.

Geologic mapping consists of mapping units (material), and geomorphic features (Hansen 2000). There are three main classes of geomorphic features: primary, secondary, and erosional. Primary features are formed during unit emplacement like lava flow structures such as levees, impact crater rims, or shield edifices. Secondary (tectonic) features occur after a unit is emplaced (i.e. faults and folds). Tectonic features can represent extensional (graben, ribbon structures, fractures) and/or contractional (folds, thrust faults) surface features. Erosional features on Venus are rare due to high surface temperatures, lack of water, and slow surface wind velocities between 0.5-1 m/s (Weitz 1993). In SAR images material units display radar-smooth areas and both primary and secondary features display lineaments.

The majority of material units on Venus consist of volcanic material, mostly basaltic in composition (Barsukov et al. 1982 and 1986). These units cover large areas across the planet and display radar-smooth characteristics. The large areas of material units show a range of radar backscatter. SAR images can vary in brightness across regions based on changes in surface roughness (Ford et al. 1993).

Primary and tectonic features on Venus appear as lineaments in the SAR data, and provide information on relative ages and surface histories. Lineaments are not all the same. When mapping it is important to be aware of patterns, spacing between lineaments, the character of the lineaments, radar gradation, and radar brightness. These lineament parameters can aid in identification of structures. The types of structures on the surface

are identified from looking at the SAR images and taking into account the positions of dark, bright, and gray lineaments in the image. Troughs have dark bands closer to the direction of illumination (Stofan et al. 1993). Ridges have bright and dark lineament pairs and can have a high degree of sinuosity along strike. Figure 2 shows two topographic shapes for surfaces and how radar interacts with each surface. Panels A and B each show a cartoon block diagram of a surface (i), the associated radar image (ii), an example SAR image (iii), and the interpreted surface topography of that SAR image (iv). In both cases A and B show ridges, however A has steep slopes and sharp boundaries between slope domains, whereas B has shallow slopes and gradational slope boundaries.

4. MAP RELATIONS

The study area is divided into seven domains (A – G) based on topography and surface roughness (Fig. 3). On Venus the surface is measured in km above and below mean planetary radius (MPR), 6051.84km (Ford and Pettengill 1992). Elevation describes features in reference to MPR. Domains, A, C, E, and F, have high elevations and high surface roughness, typical of RTT. Domains B and D lie at low elevation and contain large tracts of mostly radar-smooth material, indicative of low viscosity lava flow. Domain G lies at high elevation and includes both radar-rough and radar-smooth material, and mostly folded terrain. Domains A, C, E, and F display characteristic RTT fabric, and are collectively referred to as RTT domains. Domains B and D are collectively referred to as lowland domains. Domain G displays a different character from both RTT and lowland domains; acting like a transitional domain, but will simply

be referred to as domain G. The domains do not represent specific geologic units and served as tools in preliminary mapping.

The study area broadly displays undulating topography from north to south and the entire map area gradually decreases in elevation from north to south. Most of the study area falls into the category of mesolands, although RTT domains are higher in elevation and parts of lowland domains sit below MPR. Figure 4 displays N-S transects taken every 5° longitude eastward from 55E. Together the seven profiles show qualitative comparisons between domains. The four RTT domains each lie at least 1 km above MPR. Domain E, the northernmost domain, is topographically higher than all other domains, ~3 km above MPR. Domain F is at ~2 km above MPR, and domains A and C both lie ~1 km above MPR. Domain F bounds the western margin of the map area and domain A bounds the southern margin. Domain C crosses through the southern half of the map area with an arcuate shape, dividing lowland domains B and D (Fig. 3).

Domains B and D are both considered to be lowland domains, even though it could be argued that the area for these two domains is in the mesolands. These two lowland domains are located between two RTT domains; domain B lies north of domain A and south of domain C, whereas domain D lies north of domain C and to the south of domain E (Fig. 3). Domain D varies in elevation from 3 km in the north to 0-0.5 km in the south, and domain B varies in elevation from 1 km below MPR to 1.5 km above MPR, with a general decreasing slope from north to south (Fig. 4). Domain D sits topographically higher than domain B. Sharp topographic or structural boundaries occur between lowland domains and RTT domains.

Domain G, located between RTT domains C and F, and lowland domains B and D, rises ~1 km above MPR. Domain G displays characteristics of both RTT domains (high elevation) and lowland domains (less surface roughness), and represents an important area for further investigation. The spatial location of domain G, between multiple RTT and lowland domains (Fig. 3) is ideal for investigating the relationships between structures in RTT and lowland domains.

A large region of northern Tellus Regio was mapped at a reconnaissance scale (Plate 1). Material units and structures within the map area are described below; structural elements are categorized into primary and secondary structures. In the section following the descriptions of structures, both spatial and temporal relationships of structures within each domain are described. Target map areas highlight important relationships between structural elements, and serve to illustrate spatial and/or temporal patterns observed in the map area. Crosscutting relationships between structural elements provide information on the temporal evolution across each domain. Lastly both spatial and temporal relationships between domains are examined and aid in interpreting a geologic history of the study area.

4.1 Material Units

Large areas of radar-smooth material occur across the map area. Areas of radar-smooth material are commonly interpreted as lava fill from volcanism (Ford et al. 1993), and are referred to as volcanic plains. Lava fill covers areas of low elevation and structural lows (troughs) and in SAR images can display a range of radar-smooth tones. In the study area lowland domains contain large tracts of lava fill material. ITBs, another material unit, found mostly in RTT domains, are described below.

ITBs, generally display elongated shapes of differing radar-dark tones, and occur within RTT domains in the troughs of multiple-λ structures including folds and ribbon structures (Banks and Hansen 2000). Generally ITBs trend parallel to both the margin of the domain and long-λ folds, with elongate forms. In the study area ITBs have long axes ranging from 6-300 km and short axes from 5-30 km. Within the ITBs, secondary structures locally deform basin fill.

4.2 Structures

Structures affect and/or crosscut material units and can either be primary or secondary. Primary structures are formed during unit emplacement; examples include impact crater rims, and volcanic flow levees and flow fronts. Secondary structures occur after a unit is emplaced; examples include faults and folds. Primary structures in the map area include both impact structures and volcanic structures; primary structures generally occur within the lowland domains.

Impact crater structures include central peaks, crater rims and ejecta deposits. Impact craters are generally marked by circular to quasi-circular outlines, a raised rim, and a depth that is shallower than the crater rim diameter (Weitz 1993). The size of impact craters commonly display changes in morphology. Large craters may display multiple rings, whereas medium craters commonly display a central peak, however both large and medium crater floors are smooth; small craters display a bowl shape with a rough floor. In the study area crater structures commonly display a central radar-bright circle, with a radar-smooth floor, and a surrounding ejecta deposit of radar-bright material. Crater rims in the study area range from 5-30 km diameter; ejecta deposits

extend outward to 30 km. Six impact craters occur with the map area – one in an RTT domain, and five in lowland domains (Fig. 5).

Volcanic features include shield volcanoes, pit chains, and circular features. Shields are circular bumps interpreted to be volcanic in origin (Aubele and Slyuta 1990, Head et al. 1992, Guest et al. 1992). The shields in the study area display small diameters of 0.5-1 km, and are identified by the presence of a summit collapse pit and differences in radar backscatter with the surrounding plains (Guest et al. 1992) Shields form in clusters, covering large tracts of the lowland domains. Shields and accompanying deposited lava material together make up shield terrain (Hansen 2005). In the study area shield terrain occurs in both lowland domains, however it appears that more shields occur in domain D than in domain B. This could be based on sizes of domains and apparent visibility, and hence biased, but the general observation should be included in describing the structures.

Pit chains (Wyrick et al. 2004, Davey et al. 2013) are present in two forms; multiple circular pits that together form straight lines (appearing as a string of beads), or linear to curvilinear troughs marked by scalloped edges. Pit chains, generally elongated features, display a straight, long (up to 100 km) character, with widths of ~1-2 km. Pit chains commonly occur within both RTT domains and lowland domains, trending parallel to elongate ITBs in RTT domains; pit chains lack a preferred orientation in the lowland domains. Pit chains display steep-sided depressions and generally form from collapse from removal of subsurface support (Wyrick et al. 2004, 2010).

Circular features occur within the eastern half of domain D along with shields (Fig. 5). Circular features, generally display a singular bright circular lineament with diameters ranging from 10 to 75 km. Some circular features also display radial radar-

rough lineaments and concentric lineaments. The radial lineaments can be either ridges or fractures. The circular features occur within the eastern half of domain D along with shields. Based on sizes and morphology the circular features are interpreted as arachnoid structures (Barsukov et al. 1986, Head et al. 1992). The concentric structures are commonly irregular and arachnoids generally display a web-like pattern. Arachnoids tend to be magmatotectonic in origin (Head et al. 1992).

Secondary Structures

Secondary structures form as a result of deformation of an already emplaced unit. Secondary structures in the map area include folds, ribbon structures, graben complexes, fault scarps, wrinkle ridges, and sets of lineaments (A-F). Lineaments A-F display some characteristics of graben and fault scarps, indicating extensional structures. Each of these structural elements is described in turn below, with lineaments A-F listed in order of abundance across the study area.

Multiple wavelength folds occur across the map area. All folds display a gradational radar tonal change from bright to dark, corresponding with going from radar-facing limb to crest (Stofan et al. 1992). Long-λ folds display a curvilinear character, with wavelengths of 40 to 200 km and lengths of 90-900 km. Medium-λ folds display a curvilinear character, with wavelengths of 2-20 km and lengths of 15-120 km. Short-λ folds also display a curvilinear character, with wavelengths of 0.5-1.5 km and lengths of 2.5-60 km. Long-, medium-, and short-λ folds occur in RTT domains and are important in the formation of RTT fabric, and hence crustal plateaus (Hansen 2006). Folds also occur in the lowland domains, with wavelengths of 2-5 km, and in domain G where wavelengths vary from 0.5-2.5 km.

Ribbon structures, marked by alternating sets of bright and dark lineaments, are defined by flat-topped ridges and flat-bottomed troughs connected by steep walls (Hansen and Willis 1996, 1998). Ribbon structures are either shear or tensile opening fractures. These extensional structures display a straight character, and generally trend orthogonal to fold crests. Ribbon troughs/ridges range from 3 to 30 km long. The spacing between ridges range consistently between <0.5 and 2 km, defining a strong periodicity. The width of ribbon troughs range from <0.5 to 1.5 km and contain radar-smooth fill. Ribbon structures occur most abundantly in RTT domains, but also occur locally within RTT inliers in the lowland domains and domain G (Fig. 5).

Graben complexes are comprised of suites of oppositely-dipping normal faults that bound each side of a radar-dark elongated area (Bindschadler et al. 1992: Ghent and Hansen 1999). Due to the look-direction bias in the map area data, the majority of mapped scarps are west-facing and display a bright, straight to curvilinear character; however, east-facing fault scarps are inferred as equally dominant. Graben complexes are mapped as both individual fault scarps within the complex and the elongated shape of the complex. The multiple bright scarps together display an interwoven character within a single graben complex. The spacing between individual west-facing scarps is less than 1 km. Generally the spacing between graben complexes ranges from 10 to 45 km and in local areas graben complexes display a periodicity. The width of the graben floor varies between 2.5 and 5 km and the width of the entire graben complex varies between 2.5 and 40 km. Graben complexes range in length from 10 to 160 km and long graben complexes vary in width (i.e. Domain E). Graben complexes occur in RTT domains F, C, and E.

Fault scarps occur in domain C, and are marked by straight, single bright lineaments. Fault scarps are 5-40 km long with widths ~1 km. The spacing between scarps range from 1-10 km. Fault scarps trend parallel NW, parallel to long-λ fold crests.

Wrinkle ridges (Bindschadler et al. 1992, Banderdt et al. 1997) individually display a sinuous character, and with multiple wrinkle ridges display a polygonal pattern. Wrinkle ridges show gradational changes over crests, similar to folds. Wrinkle ridges occur commonly within radar-smooth material (ITBs and lowlands) and cover large areas. Wrinkle ridges occur predominately in domains B and D, however wrinkle ridges occur locally in ITBs within domain A, and within the RTT fabric in domain C (Fig. 5).

Lc, which occur within RTT domains (A, C, and E) and lowland domains (B and D), are marked by single, bright lineaments. Lc are most abundant in domain B and A, occurring across each domain; these lineaments occur locally in domain D, C, and E (Fig. 5). Lc generally trend NE, and display an overall anastomosing character, appearing in bundles. Individual lineaments appear straight, ranging from 2-30 km in length; spacing between lineaments is generally <1 km. Individual dark lineaments can accompany and parallel bright lineaments, although due to the radar-look direction bright lineaments are easier to distinguish. The width between bright and dark lineaments varies from 0.5-1.5 km; because SAR data are left look, producing bright lineaments to the right of dark lineaments, these structures mark narrow troughs and are interpreted as extensional structures.

Lb, which occur in domains D and E (Fig. 5), are marked by single, bright lineaments; they display an overall anastomosing character and trend NW. Lb can also show dark lineaments that trend parallel to bright lineaments, however the majority of Lb

are identified by bright lineaments based on look direction. Individual lineaments, ranging from 5-60 km in length, appear straight, with spacing between 1-2 km. The width between bright and dark lineaments is generally quite small, down to the resolution of the SAR data (<0.5 km). Lb display similar characteristics as Lc, however Lb are more locally developed and trend NW.

Ld, which occur in domains B and F (Fig. 5), are marked by paired bright lineaments; they display a straight and consistent character. Each pair of bright lineaments ranges from 2 to 100 km in length: spacing between lineament pairs is between 2-4 km. The width between paired bright lineaments, generally ~1 km, stays consistent across domain B. Between pairs of bright lineaments, radar-dark material occurs. The interaction between the trend of lineaments and the radar look-direction can change the appearance and character of Ld. When Ld trend parallel to the radar look-direction the lineaments appear as bright pairs with the above characteristics, which is the case for domain B, however when the lineaments trend at an angle to the radar look-direction Ld display characteristics similar to Lc, with paired bright and dark lineaments. Similar lineaments were mapped by DeShon et al. (2000); these workers interpreted the double lineament character as fractures with topographically raised edges, and interpreted the fractures to record extension, based on a lack of shear displacement along the fractures and the consistent straight boundaries.

Lf, which occur in domain D (Fig. 5), are marked by paired bright lineaments; individually they display a straight, consistent character, generally trending E-W. Across the domain Lf display a curvilinear and fibrous character, and look to be confined within local, anastomosing strips. The lengths of Lf range from 5-100 km; spacing between sets

of bright pairs is ~1-2 km. The width between bright pairs of lineaments is generally <0.5 km.

La, which occur only in domain F (Plate 1), are marked by paired bright lineaments, spaced ~1-1.5 km; they display an interfingering character and generally trend E-W. La occur in large ITBs within domain F, generally crosscutting basin fill and forming after fill of the ITBs. La, Ld, and Lf, although similar, are distinguished and mapped separately based on lineament characteristics such as spacing between bright lineaments and abundance.

Le, which occur in domain B, are marked by single, short, bright lineaments; they display a straight character and generally trend N-S. Le vary in length from 1-4 km, and display a consistent spacing of ~1 km.

4.3 Domains

As previously noted, the study area is divided into seven domains (A-G). The general characters of each domain are described below including what structures are present. Which structures occur in multiple domains, and structural orientation of structures between domains, are of particular importance and will later be referred to in a discussion of the spatial relationships between domains. Domain F, an organized RTT domain that displays characteristic RTT fabric and patterns between structures, is described first.

4.3.1 DOMAIN F

Domain F, located in the western portion of the study area (Fig 3), sits topographically high and includes mostly RTT, which displays a complex, but organized structural fabric. Detailed geologic mapping of domain F reveals coherent patterns of

structural elements defining an organized RTT package and relatively simple geometric relationships. Elements of domain F include ITBs, folds, ribbon structures, graben complexes, and La and Ld.

ITBs, present throughout the domain, generally trend NW, with long axes ranging from 20-300 km; ITBs occur within medium-λ fold troughs, and along the limbs of long-λ folds (Fig. 5). ITBs are larger to the south than the north. Along the northern and eastern margins, ITBs occur sporadically.

Long-λ folds with wavelengths ~80 km, and lengths between 200-350 km, trend NW, parallel to ITBs. Medium-λ (2-10 km) and short-λ (0.5-1 km) folds trend parallel to long-λ fold crests. Short-λ folds display more variability in trend than either long- or medium-λ folds, trending E-W in the north. Both medium- and short-λ folds are most abundant in the central part of domain F, and occur sporadically along the northern and eastern margins (PLATE1). Short-λ folds occur on the crests and limbs of both medium- and long-λ folds.

Ribbon structures and graben complexes generally trend NE, orthogonal to local trends of fold crests. Ribbon structures typically trend orthogonal to short-λ fold crests, NE in the center of the domain and N-S to NW in the north. Ribbon structures are ~20 km in length, 0.5-1.5 km wide, and have spacing between same facing scarps of 1-2 km. Ribbon structures become sparse in the northern portion and along the eastern margin of domain F (Fig. 5). Graben complexes trend NE, parallel to ribbon structures and orthogonal to long- and medium-λ fold crests. Graben complexes are 20-90 km in length, 2.5-40 km wide, and have spacing between complexes of 10-20 km; they occur

pervasively in the southwestern half of the domain (PLATE1) with less graben complexes to the north and east.

Domain F also contains La and Ld. La occur in the southwestern portion within large ITBs. Ld occur mostly in local areas in the north and along the eastern margin (Plate 1). Ld vary in length from 30-180 km and trend NW.

Target map F1 illustrates the characteristic RTT fabric, displaying multiple-λ folds, ribbon structures, graben complexes and ITBs, together forming a complex, but coherent structural fabric marked by simple patterns (Fig. 6). Domain F displays the most coherent RTT fabric and F1 serves as an important starting point for identifying RTT. F1 also shows local flood deposits between all structures (folds, ribbon structures, and graben complexes).

Similar temporal relationships occur across domain F. Ribbon structures cut short-λ folds, and both medium- and long-λ folds cut ribbon structures. Graben complexes cut long-λ folds and ITBs occur in structural lows of multiple-λ structures including folds and ribbon structures. Ld cut the folds and ribbon structures along the eastern boundary of domain F, and Ld cut large ITBs in the south. La cut large ITBs in the southern region of domain F. Some graben complexes cut La, forming after or representing reactivation of a previously formed structure.

The wavelength of folds and spacing between extensional structures allows for calculation of layer thicknesses, useful in examining temporal relationships between structures. Using empirical fold wavelength-to-layer thickness ratios of 3-6 and ribbon structure wavelength-to-layer thickness ratios of 2-4 (Hansen 2006) first order approximations for layer thicknesses are calculated. The layer thickness is 0.125-0.25 km

during short-λ fold formation, 1-2 km during medium-λ fold formation, and 13-26 km during long-λ fold formation. During ribbon structure formation layer thickness is 0.375-0.75 km and during graben complex formation layer thickness is 3.75-7.5 km. As the layer thickened, the spacing/wavelengths of structures also increased. Short-λ folds form with the thinnest layer, and therefore formed at the earliest time, followed by ribbon structure formation, broadly overlapping and forming synchronously with short-λ folds. With progressive deformation and cooling, the layer thickens, and medium- and long-λ folds form. During the formation of longer-λ folds, earlier formed shorter-λ folds get carried "piggyback" by the long-λ folds. Hansen (2006) provides a detailed discussion of the timing of short- to long-λ fold formation.

The presence of short-λ folds at the crests of longer-λ folds might occur by synchronous formation of two compositionally different layers, i.e. parasitic folds. This is not the case for Venus, which is thought to have a homogenous basaltic composition. The presence of radar-smooth fill at the crests of long-λ folds cannot be explained with parasitic folds, but can be explained with an increasing layer thickness and continuous volcanism. During short-λ fold formation volcanism fills topographic lows with radar-smooth material. As the layer thickens and the wavelength of structures increases, the local topographic lows of short-λ folds, now reside on the crests of long-λ folds.

4.3.2 DOMAIN C

Domain C, located in the central portion of the study area (Fig. 3), sits topographically high relative to adjacent domains, and it includes mostly RTT. Domain C has an arcuate shape going from the southeastern corner to the center of the map area. In the middle of domain C an area of low elevation, radar-smooth material is present, along

with a high concentration of Lc. Typical RTT fabric marks the western portion of domain C, whereas the eastern portion of domain C displays RTT fabric in patches, along with topographically low, yet radar-rough, areas.

ITBs, present throughout the domain, generally trend parallel to the arcuate shape of the domain, E-W in the northern portion and NW in the southeastern portion of the domain (Fig. 5). Long axes range from 6 to 90 km in length, and ITBs occur within medium-λ fold troughs, and along the limbs and crests of long-λ folds.

Long-λ folds with wavelengths ~40 km and lengths of 225-525 km, trend parallel to ITBs (Fig. 5). Medium-λ (5-15 km) and short-λ (0.5 km) folds generally trend parallel to long-λ fold crests. In local areas of domain C, just east of the middle radar-smooth area, medium- and short-λ fold crests trend E-W, roughly orthogonal to long-λ fold crests. These trends are parallel to fold crests on the western side of the radar-smooth area. Short- and medium-λ folds occur on the crests, troughs and along the limbs of long-λ folds; short-λ folds also occur along the crests and limbs of medium-λ folds with parallel trends.

Ribbon structures and graben complexes trend NW above ~54°N and NE below 54°N (Fig. 5). These structures generally trend orthogonal to short-λ fold crests. Ribbon structures are 5-30 km long and have spacing between same facing scarps of 0.5-1 km. The width of ribbon floors is at the resolution of the SAR data. Ribbon structures are abundant west of the radar-dark area, but to the east they occur in clusters. Graben complexes are 10-35 km long, smaller than 5 km wide, with inter-complex spacing of 20-45 km; they occur mostly west of the radar-smooth area.

Lc trend NE and occur pervasively in three distinct sections of domain C. Lc are 2-30 km long, with <1 km spacing between same facing scarps. Two of the sections containing Lc occur east of the radar-smooth area and are located south of 54°N; the third section is farther north in the radar-smooth area itself (Fig. 5). The two sections east of the radar-smooth area occur at lower elevation than the surrounding RTT fabric, although the regions display radar-rough material. Within these sections Lc either are the only structures visible or they crosscut previous structures.

Target map areas C1 and C2 (Fig. 7 & 8 respectively) display relationships between structures in domain C. C1 shows areas with at least two episodes of ITB formation. The older ITBs have: a lighter-grey radar tone, more structures overprinting them including ribbon structures, and occur along medium-λ fold crests. The younger ITBs show: darker radar tones and fill in the troughs of medium-λ folds. C1 shows RTT fabric, although the structural patterns are not as recognizable as in domain F, and only the radar-facing scarps of ribbon structures are visible (Fig. 7). C2 (Bigfoot) shows a difference between RTT fabric in the western half, and RTT fabric overprinted by Lc in the eastern half (Fig. 8). RTT fabric displays sets of periodically-spaced ribbon structures and orthogonal folds, whereas in the eastern half of the map area structures trend NE. Lc display an anastomosing character and cross cut medium-λ folds. The fault scarps are also illustrated in figure 8, and occur late, cutting previously formed RTT fabric. The temporal relationships between the fault scarps and Lc are not easily visible.

Domain C displays similar temporal relationships to domain F. Ribbon structures cut short-λ folds, and both medium- and long-λ folds cut ribbon structures. Graben complexes cut medium-λ folds. Domain C, displays sections of Lc, that cut all previous

structures. Within the radar-smooth, topographic low section of domain C, Lc cut the radar-smooth material. East of this radar-smooth area, two sets of Lc cut RTT fabric. Domain C has pitchains, as well as wrinkle ridges in local areas along the northeastern margin (Plate 1) that both cut RTT fabric.

The progressive increase in layer thickness calculated from the wavelengths and spacing of structures, provides a similar conclusion to that of domain F; short-λ structures formed first, followed by longer-λ structures. The layer thickness is 0.08-0.167 km during short-λ fold formation, 1.67-3.33 km during medium-λ fold formation, and 6.67-13.3 km during long-λ fold formation. During ribbon structure formation the layer thickness was 0.1875-0.375 km, overlapping and occurring synchronously with short-λ fold formation. The layer thickness during graben complex formation was 8.125-16.25 km, which broadly overlaps with long-λ fold formation. ITBs form throughout the formation of structures and fill the topographic lows of structures at the time of deposition.

4.3.3 DOMAIN A

Domain A located in the southern portion of the study area and continuing to the south outside the study area (Fig. 3), sits topographically high relative to domain B to the north, and it includes mostly RTT. Some structures that comprise RTT fabric (i.e., multiple-λ folds and ribbon structures) are less abundant than RTT within domains F and C, however structural patterns emerge as illustrated in the geologic maps.

ITBs, present throughout the domain, generally trend NE. Long axes range from 15-60 km and occur along the limbs and in the troughs of long-λ folds.

Long-λ folds with wavelengths between 70-200 km and lengths between 90-400 km, trend E-W parallel to the northern margin of the domain (Fig. 5). Medium-λ (7-15 km) folds trend E-W, parallel to long-λ folds; however short-λ (~0.5 km) folds generally trend NE. Medium-λ folds occur across domain A, whereas short-λ folds occur locally within domain A (PLATE1).

Ribbon structures trend NW, orthogonal to short-λ fold crests (Fig. 5). Ribbon structures are 3-5 km long with ~1 km spacing between same facing scarps. Ribbon structures occur more abundantly in the western portion of domain A: they are commonly overprinted by Lc. Lc occur pervasively throughout domain A and generally trend N-S. Lc are 5-30 km long with ~1 km spacing between same facing scarps. Lc mostly occur in the northern portion of domain A, and become sparse to the south (Fig. 5).

Target map A1 displays the pervasiveness of Lc within an RTT domain (Fig. 9). Map A1 shows orthogonal geometric relationships between short-λ folds and ribbon structures, and aids in recognizing the crosscutting relationships between structures. Short-λ folds are crosscut by ribbon structures.

In domain A short-λ folds are crosscut by ribbon structures. Medium- and long-λ folds cut ribbon structures, and all-λ folds and ribbon structures are cut by Lc. The layer thickness is 0.083-0.167 km during short-λ fold formation, 1.83-3.67 km during medium-λ fold formation, and 22.5-45 km during long-λ fold formation. During ribbon structure formation layer thickness is 0.25-0.5 km. Similar to domains F and C, domain A shows short-λ fold forming first, broadly synchronous with ribbon structures, and followed by the formation of medium- and long-λ folds. ITBs, sitting at the crests, along the limbs, and in the troughs of long-λ folds, indicate that volcanism occurred synchronously

throughout the formation of structures and the progressive cooling and thickening of the layer. Lc cut all types of structures in domain A, and occurred after the RTT fabric formed and was in its current spatial location.

4.3.4 DOMAIN E

Domain E, the largest RTT domain sits topographically high; it is located in the northern most portion of the study area, and continues northwest outside of the map area (Fig. 3). The majority of domain E is comprised of ITBs, multiple-λ folds, ribbon structures, and graben complexes, although areas within domain E contain Lb, Lf, and Lc.

ITBs, present throughout the domain, generally trend NW, with long axes ranging from 70 to 180 km. They occur along the limbs and in the troughs of long-λ folds (Fig. 5).

Long-λ folds with wavelengths of 60-160 km and lengths >450 km, trend roughly E-W. Medium-λ (5-20 km) and short-λ (1-1.5 km) folds generally trend parallel to long-λ folds, although short-λ folds display variability in trend from E-W to NW to NE. Medium- and short-λ folds occur across domain E (Plate 1).

Ribbon structures and graben complexes generally trend N-S, orthogonal to short-λ fold crests. Ribbon structures are 5-30 km long with 1 km spacing between same-facing scarps. Ribbon structures are sparse in the eastern portion of domain E (Fig 5). Graben complexes are 30-160 km long, 5-35 km wide, and have spacing between complexes of 30-40 km. Graben complexes become less abundant from west to east across domain E.

Lb represent the major structural element along the eastern margin of domain E (Fig. 5). These lineaments trend NW and continue into the lowland domain D to the

south. Just to the east of the center of domain E, Lc trend NE. Lf trend E-W, in parts of the southern portion of domain E.

Target map area E1 illustrates temporal relationships between structural elements in domain E (Fig. 10). Ribbon structures cut short-λ folds and graben complexes cut ribbon structures. Graben complexes display a somewhat regular spacing between complexes and get wider as they cut long-λ fold crests.

Domain E shows similar temporal relationships between structures as the other three RTT domains (F, C, and A). Across the domain short-λ structures are crosscut by longer-λ structures. Layer thickness is 0.167-0.33 km during short-λ fold formation, 2.083-4.167 km during medium-λ fold formation, and 18.3-36.67 km during long-λ fold formation. During ribbon structure formation the layer is 0.375-0.75 km thick, the same thickness during short-λ fold formation. As layer thickness increases the wavelength and spacing between structures also increases.

4.3.5 DOMAIN B

Domain B, located in the southern half of the study area, is surrounded by RTT domains, with domain F to the west, domain C to the north and east, and domain A to the south (Fig. 3). Domain B sits topographically lower than its surrounding domains and is mostly radar-smooth, although both topographic variability and radar-rough areas are present within the domain. Detailed geologic mapping reveals structural elements across the domain, including local RTT packages and shield terrain.

Long-λ folds occur across domain B, and generally trend parallel to domain margins; folds trend NW in the east, and trend NE in the west (Fig. 5). Long-λ folds with wavelengths >200 km, are ~300 km long. Wrinkle ridges occur across the domain but are

most abundant to the southwest, where they display a polygonal pattern. Wrinkle ridges consist of two sets of ridges that trend NW and NE, roughly orthogonal to one another. Away from the southwest part of the domain the wrinkle ridges lose the polygonal pattern and form one set of ridges over the other. To the northwest the NW trending set of wrinkle ridges prevails, and to the northeast the NE set occurs. Shield terrain occurs most abundantly in the southwestern region of the domain, along with the polygonal patterned wrinkle ridges (Plate 1). The southwestern region lies at the lowest elevation, and appears to be the most radar-smooth area within domain B.

Along with wrinkle ridges, Lc and Ld dominate the majority of domain B (Fig. 5). Lc trend NE across the domain, occur in bundles and display an anastomosing character. Lc are 2-30 km long with the spacing between same-facing scarps at the resolution of the data. Ld generally trend E-W, however along the eastern and western margins they trend NW. Ld are 2-100 km long with 2-4 km spacing between paired bright lineaments. Target map areas B1 and B2 illustrate the character of domain B lineaments and crosscutting relationships.

Target map area B1 mainly illustrates Lc (Fig. 11) and target map area B2 mainly illustrates Ld (Fig. 12). In each target area multiple lineaments occur; each area displays different characteristics. For example in Map B1 (Fig. 11) Ld occur between dense, fibrous strands of Lc, and show a paired bright lineament character. Lx, a single bright lineament, trends E-W. The trend of Lx is similar to Ld, and at this scale the two appear to have a different character (single bright lineament (Lx) versus paired bright lineaments (Ld)); however as noted above, Ld locally display a single bright lineament character. Even though area B1 highlights the anastomosing character of Lc, information about

other lineaments is revealed. Map B2 (Fig. 12) displays Ld and their consistent spacing and paired lineament character. This map area is also the only region that illustrates Le and their spatial relationships to other structures. Ly (anastomosing character) differs from Lc (straight character) at this scale, however as noted above Lc can display an anastomosing character. Lx and Ly are mapped in these two target areas in an effort to illustrate how the same structures can display different characters at different scales.

Local kipukas of RTT occur across domain B, occurring most common along the northern and western margins (Fig. 5). RTT kipukas typically sit topographically higher than their surroundings. Kipukas along the northern margin of domain B display folds (wavelengths of ~2.5 km) that trend parallel to the domain margin, generally E-W. Along the western margin of domain B, kipukas display sets of lineaments that trend orthogonal to one another; one set trends NE with spacing ~2 km, the other set trends NW with spacing <1 km. Kipukas in areas where Lc occur abundantly, display a fibrous character and generally show abrupt changes in grey tone compared to their surroundings. Kipukas occur along the crests, troughs, and limbs of the long-λ folds in domain B.

Across domain B similar temporal relationships between structures occurs. Generally Lc cut Ld, and both are crosscut by wrinkle ridges. There are some areas in the eastern region of domain B where Ld cut Lc, indicating that Lc broadly form synchronously with Ld, or that Ld were reactivated during Lc formation. Domain B displays RTT kipukas that are cut by one or both sets of lineaments. The southwestern region of domain B displays RTT kipukas that are not deformed by Lc or Ld. In this area of domain B, polygonal patterns of wrinkle ridges cut over mostly radar-smooth base material.

4.3.6 DOMAIN D

Domain D, located in the northern half of the study area, lies between RTT domain E to the north and RTT domain C to the southeast and domain G to the southwest (Fig. 3). Domain D sits topographically lower than surrounding domains, however the northern half of domain D sits much higher than the southern half (Fig. 4). The northern half of domain D also contains the majority of Lf and kipukas of RTT. Domain D also includes wrinkle ridges, Lb, and abundant volcanic features including shields and arachnoids (Plate 1).

Lf trend E-W, with lengths from 2-100 km and 1-2 km spacing between paired bright lineaments. Lf occur in E-W trending bands across the northern half of domain D, where elevation is above ~1km. Kipukas of RTT display radar-rough and elevated terrain. Some kipukas preserve ribbon structures and fold crests oriented orthogonal to one another.

One set of wrinkle ridges, trending N-S, occurs in domain D. Wrinkle ridges occur in the western half of the domain just north of domain G. Lb trend NW, with lengths 5-60 km and 1-2 km spacing between same-facing scarps. Lb occur mostly in close proximity to arachnoids in the eastern portion of domain D, where volcanic features are more abundant.

Long-λ folds occur in domain D, with the majority trending E-W, and one long-λ fold crest trending NE. The NE trending long-λ fold crest connects to an arachnoid feature and appears to be associated with volcanic deformation, whereas the other long-λ folds trend parallel to both Lf and folds associated with RTT kipukas.

Target map area D1 illustrates RTT kipukas and other structures that comprise domain D (Fig. 13). Ribbon structures trending orthogonal to folds comprise RTT kipukas, along with high radar-roughness. Folds associated with RTT kipukas trend E-W, parallel to Lf. Lb crosscut Lf, and wrinkle ridges crosscut both Lb and Lf.

The temporal relationships between structures in target map area D1, broadly characterizes the temporal relationships across the entire domain. RTT kipukas show areas without Lf, and areas where lineaments F crosscut the kipukas. Lb cut both Lf and RTT kipukas, as well as the folds associated with RTT kipukas. Wrinkle ridges across domain D cut Lf, however crosscutting relationships between Lb and wrinkle ridges are difficult to observe.

4.3.7 DOMAIN G

Domain G is located between RTT domains F to the west and domain C to the east and lowland domains D to the north and domain B to the south (Fig. 3). Domain G, shaped like a capital letter Y, is dominated by folds that trend N-S in the southern portion and E-W in the northern portion; fold trends mimic the "Y" shape of the domain (Fig. 5). These folds have wavelengths from 0.5-2.5 km with lengths of 20-120 km. The wavelength of folds corresponds to a layer thickness of 0.25-0.5 km. The majority of the terrain comprising domain G is folded terrain with local exposure of RTT kipukas.

In the northern portion of domain G ribbon structures occur along the crests of some folds. Target map area G1 illustrates spatial relationships between structures within domain G (Fig. 14). The ribbon structures trend NE, roughly orthogonal to the E-W trending folds. Within domain G, RTT patches occur, with internal structures similar in character and trend to structures in the adjacent RTT domains. Most RTT kipukas display

folds that trend NE and ribbon structures that trend NW. These orientations are the same as the orientations for short-λ folds and ribbon structures in the western portion of domain C. There is a sharp boundary between kipukas of RTT with domain C structural affinities and the eastern margin of domain F, marked by N-S trending folds. Between some of the RTT kipukas with domain C structural affinities N-S trending folds also occur.

Domain G shows temporal relationships similar to both RTT domains and lowland domains, however impact craters aid in discerning relationships between structural elements and the relative timing between impact events. In RTT kipukas ribbon structures cut short-λ folds and medium-λ folds cut ribbon structures. Ld cut the N-S trending folds and some RTT kipukas in domain G, indicating that Ld occurred after the formation of RTT kipukas and the folds. The impact crater in the center of domain G sits topographically lower than the surrounding folded terrain and the suites of folds and Ld continue right to the boundary of the crater rim. The crater truncates the folds and Ld, indicating that the impact event happened after formation of both the folds and Ld. The impact crater north of domain G, displays an ejecta deposit with a distinct flow. The flow occurred when the ejecta material was buttressed by an elevated region; hence this impact crater formed after the formation of Domain G and its folded terrain.

4.4 Spatial and temporal relationships between domains

The spatial and temporal relationships between domains and how domains relate to one another are important concepts in addressing the following two research questions: what is the northern extent of Tellus Regio, and what are the interactions between crustal plateaus and lowlands? I examine inter-domain relations in three different regions; in

each region I address the two research questions. In the first region I examine relations between domains C, A, and B; in the second region I examine relations between domains C, F, and G; and in the third region I examine relations between domains E and D.

4.4.1 REGION 1

Domain B lies between RTT domains A and C (Fig. 3). Domains A and C show similar orientations of structures, fold crests trending parallel to each domain margin, generally E-W, and ribbon structures trending N-S (Fig. 5). Domain B contains RTT kipukas (mostly in the north) with RTT fabric orientation similar to those of domain C. In addition, long-λ folds along the eastern margin of Tellus Regio (to the south) continue north and merge into parallelism with the long-λ folds in domain C. The similarities of structures and their orientations within domains A and C indicate that domains A and C are genetically related, and could be one connected RTT terrain that continues beneath surface deposits in domain B (Fig. 15). The similar trends of long-λ folds along the eastern margin of Tellus Regio and domain C indicated that these two regions could be related as well. The RTT kipukas within domain B represent 'basement exposures' of RTT fabric, that escaped burial, and which are mostly undisturbed from the other tectonic structures in domain B. The similar orientations of structures between southern Tellus Regio, and domains A and C, indicate that Tellus Regio encompasses domains A, B, and C, and that the northern boundary of Tellus Regio extends north to include all of domain C.

Domain B could represent an area of partial crustal plateau collapse or an area of a crustal plateau that did not achieve the same amount of rise in elevation across the entire domain. Ld cut Ld in domain B, and in domains A and C, Lc cut pre-existing folds

and ribbon structures. Both Lc and Ld are extensional structures, providing possible evidence for crustal plateau collapse, however Lc appear in three distinct zones where these lineament suites cut domain C (Fig. 5). If domain B was once elevated to the same local level as the regions in domains A and C, the extensional strain should be roughly equal across the area, and not be confined into three sections. If however, domain B never resided at the same local elevation as domains A and C (perhaps due to domain B representing a thinner rheological layer), then extensional strain across domain C (the thicker of the two) might be partitioned into distinct sections, with the spacing between extensional zones representing a proxy for domain-layer thickness.

4.4.2 REGION 2

Domain G separates domains C and F, overlapping portions of both domains and the boundary between these two domains (Fig. 3). The structural elements in domains C and F show nearly opposite orientations. In domain C, fold crests trend E-W to SW in the west and ribbon structures trend N-S to NW in the west. In domain F, fold crests that trend NW and ribbon structures that trend NE. Within domain G, the orientation of structures from domain C and the orientation of structures from domain F meet and form a sharp divide (Fig. 14). The opposing orientations of structures indicates that domains C and F are separate regions, and likely evolved and deformed independent from one another; that is, these two RTT domains are not genetically related. This does not however exclude the possibility of the synchronous evolution of both domains. N-S trending folds within domain G, consisting of radar-smooth and rough material, divide the two domains. The RTT kipukas to the east of this division show affinities to structural orientations in domain C, indicating that these RTT kipukas are related to domain C (Fig.

14). Thus, the western extent of domain C continues until it reaches the eastern margin of domain F, and RTT fabric lies beneath the layer which hosts the folds and folded terrain in domain G (Fig. 16).

The area between domains C and F is an important area located between two separate large tracts of RTT fabric. Based on the structural relationships noted above I interpret domain G to be a suture zone, forming from the collision between domains C and F. This suture zone consists of a material unit, which formed after the RTT fabric of both domains C and F, and which was folded during or after emplacement of folded terrain material, with fold crest trending orthogonal to the relative direction of collision of domains C and F. The folds in domain G are cut, in turn, by Ld indicating that the collision and suturing of domains C and F occurred before the extensional deformation recorded in domain B. Domain F encompasses a separated RTT unit than that of domain C (and by association domains A and B as noted above) and is not part of Tellus Regio based on tectonic patterns.

4.4.3 REGION 3

Domain E, the northernmost domain in the study area (Fig. 3), continues to the north and west outside of the study area. Domains E and D have a sharp surface roughness boundary, separating distinct RTT fabrics in domain E, from more radar-smooth material in domain D. The topographic boundary between the two domains is gradational with the steepest topographic change residing not at the surface roughness boundary, but farther to the south within domain D (Fig. 3 & 4). This elevation change serves as a topographic boundary within domain D dividing the domain into northern and southern subdomains. The northern subdomain shows more Lf and RTT kipukas with

fold trends parallel to the RTT fold trends along the margin of domain E. Elevation in this area varies from 1-2.5 km above MPR. The southern subdomain displays radar-smooth material and volcanic features such as arachnoids (Fig. 5). The southern subdomain differs from the northern subdomain based on both elevation and characteristic structures. The southern subdomain lies at ~0.5 km above MPR, and marks a sharp topographic boundary between the northern subdomain of domain D to the north and domain C to the south.

Temporal relationships between structures in domains D and E aid in understanding the evolution of this area. Lf and Lc cut the RTT fabric of domain E, and therefore formed after the formation of domain E RTT. Lb cut Lf and areas in the eastern part of domain E. Lb are associated with volcanism relating to the arachnoids and other late forming structures. Wrinkle ridges are the last structures to form, cutting both lineament suites Lf and Lb. Lf and RTT kipukas trend parallel to the southern margin of domain E. Lf and Lc, both extensional structures, occur along the southern margin of domain E.

Although domain E and domain C host RTT fabrics with near parallel fabric trends, the sharp topographic boundary in the southern subdomain of domain D, noted above, is here taken as the northern limit of Tellus Regio. In addition to this sharply defined topographic trough, which also parallels the boundaries of domains C and E, also coincides with structural characteristics of the northern and southern subdomains of domain D. Domain D does show similar characteristics as domain B, however these similar structures only occur in the northern half of domain D. The structures in domain

B occur across the domain. Domain E also continues hundreds of km farther north and west. Tellus Regio does not continue past domain C.

So how is Tellus Regio defined? Tellus Regio extends north to domain C and includes domains A and B (Fig. 17). The opposing structural trends between domains C and F, and the folded terrain of domain G between these domains, indicates that domains C and F formed separately and were later juxtaposed with one another. Domain D is divisible into northern and southern subdomains, based on topographic and structural characteristics. The northern subdomain displays structural similarities to domain B, and hence could be part of a crustal plateau, whereas the southern subdomain displays volcanic features and lies at low local elevation, and is here interpreted to represent a topographic boundary between two different crustal plateaus, marking the northern boundary of Tellus Regio to the south.

5. EVALUATIONS OF CRUSTAL PLATEAU HYPOTHESES

Structural and geologic mapping of the study area has provided both spatial and temporal relationships between structures within domains, and across the map area. Many spatial and temporal relationships occur throughout the study area and in particular among the RTT domains. These relationships, listed below, serve as requirements for crustal plateau formation.

1. The structures that occur in RTT domains include short-, medium-, and long-λ folds, ribbon structures, graben complexes, and ITBs and flooded deposits at multiple current elevations. Short-λ folds crests trend orthogonal to ribbon structures across the study area. All of the RTT domains in the study area also show late deformation, mostly

extensional structures. Any hypothesis needs to address the presence of all of these structures and their spatial relationships (i.e. orthogonal folds and ribbon structures).

2. The wavelength of folds and the spacing between extensional structures increases with time. The formation of such small-λ structures early on indicates that they formed during a period with a high geotherm and with an exponential decrease in viscosity with depth (Hansen 2006). Hypotheses need to address this increase in structural wavelength or spacing through time in order to fully explain the structures mapped.

3. Volcanism occurs across the study area, and in RTT domains volcanic deposits occur at multiple elevations. They occur in the structural lows of many different structures including all-λ folds, ribbon structures, and graben complexes. Volcanism also occurs between RTT domains and during late extensional deformation in areas around RTT domains.

All crustal plateau formation hypotheses need to address these three concepts; the presence of all structures and their spatial relationships (i.e. orthogonal folds and ribbon structures, an increase in structural wavelength or spacing through time, and the presence of volcanic deposits at multiple elevations). The observed and mapped collision and suturing between separate plateaus should also be addressed or possible with each hypothesis.

5.1 Mantle Downwelling Hypothesis

In the mantle downwelling hypothesis a crustal plateau forms due to crustal thickening by lower crustal flow accretion, driven by a mantle downwelling or coldspot. Crustal material, drawn toward the region of downflow, begins to deflect downward,

causing surface deformation and the formation of a circular lowland and contractional concentric structures. The crust thickens with continued pooling of ductile lower crust above the downflow, leading to the area directly above the downflow rising isostatically, creating a crustal plateau. As downwelling subsides, the center of the plateau spreads under its own weight creating extensional features. The structures on top of the plateau decrease in elevation, however due to a thickened crust the plateau remains elevated.

The mantle downwelling hypothesis calls on a coldspot and therefore a cold geothermal gradient as the mechanism for crustal plateau formation. A cold geothermal gradient directly contradicts requirement 2, above, and the fact that both short-λ folds and ribbon structures need a high geothermal gradient and a decrease in viscosity between layers to form. This hypothesis does not account for relationship 3, synchronous volcanism and structural formation seen in this study. The mantle downwelling hypothesis cannot account for the observations in the study area, and therefore the requirements for crustal plateau formation.

5.2 Mantle Upwelling Hypothesis

The mantle upwelling hypothesis calls for a mantle plume and resultant partial melting in the upper mantle and subsequent magmatic underplating as the mechanism to accommodate crustal thickening during crustal plateau formation. As the mantle plume rises, the crust heats up and uplifts causing extensional structures to form first. Magmatic underplating at depth leads to thickening of the crust, resulting in isostatic uplift of the plateau. As the area cools local shortening occurs and the plateau remains uplifted due to a thickened crust.

In the mantle upwelling hypothesis ribbon structures are the first structures to form, and would not cut any other structure, a direct violation to the observed temporal relationships between short-λ folds and ribbon structures. Even though this hypothesis describes the layer thickening over time, it does not account for the formation of longer-λ folds through time, geological requirement 2 above. In this hypothesis there is a higher geothermal gradient but not an exponential decrease in viscosity with depth. Mantle upwelling does not address all of the requirements for crustal plateau formation.

5.3 Pulsating continents hypothesis

The pulsating continents hypothesis calls for thick crust due to the formation of concentric fold and thrust belts. In this hypothesis an initial area of low-density crust that has survived a global subduction event and displays previous extensional structures (ribbon structures), is compressed horizontally due to a density driven inversion. This process causes shortening of the surface and the formation of concentric thrust faults and folds along the margins of an evolving plateau. As a result of crustal thickening, folding and thrust faulting occur in the center of the plateau. This thickened crust causes isostatic uplift and the plateau to become elevated. At a later time, the generation of new lithosphere changes the force balance, leading to gravitational collapse and the formation of extensional structures. The new rigid lithosphere surrounding the plateau stops total plateau collapse, and preserves the crustal plateau as it is observed today. During partial plateau collapse extension causes radial graben to form along the margins of the plateau and concentric contractional structures form in the adjacent plains. It is during this extensional stage that intratessera volcanism occurs. Folds generally predate extensional

structures and the entire process repeats, progressively accreting more material to the edges of a plateau.

This hypothesis does include intratessera volcanism, but this volcanism happens toward the end of the plateau formation and not throughout the formation of RTT fabric, contradicting geological requirement 3. Furthermore, in the map area there is a lack of radial graben in the plateau and concentric contractional structures in the adjacent plains, contradicting the spatial relationships of structures summarized in requirement 1. This hypothesis does not predict nor accommodate the regional extent of both short-λ folds and ribbon structures. The pulsating continents hypothesis does not address parts of all three requirements and therefore cannot account for crustal plateau formation.

5.4 Lava-Pond and Bolide Hypothesis

The lava-pond and bolide hypothesis calls for crustal plateau formation from the processes and evolution of a giant lava pond. In the hypothesis this lava-pond is created from an external catalyst, a bolide impact. The impact creates massive partial melting which makes its way to the surface, forming a huge lava pond. The geothermal gradient is so high that the lava pond is liquid with the solidifying surface being a solid. As the pond cools, and convection continues in the liquid pond, the cooler surface 'scum' of the pond is deformed by multiple short-λ contractional and extensional structures trending orthogonal to one another. As this pond "scum" solidifies it thickens with time and longer-λ structures are created. At depth, beneath the lava pond (which resides on a crustal layer), mantle melt residuum is depleted and more buoyant than mantle material that did not undergo massive partial melting; low density mantle melt residuum causing the entire lava pond to become uplifted isostatically. Because the depleted mantle melt

residuum root lies in the ductile part of the mantle, two paths for evolution can occur: 1) the root is stripped away by mantle convection leading to collapse of the plateau, or 2) the cooling of the lithosphere trapped the root in place, and the plateau remains topographically high.

In this hypothesis short-λ folds and ribbon structure formation broadly overlap in time with trends orthogonal to one another, and longer-λ structures form with increasing layer thickness, thus satisfying the first two geological requirements. The lava pond has the high geothermal gradient and the decrease in viscosity with depth needed for the formation of multiple wavelength folds, and continued volcanism associated with crustal plateaus, as given by geological requirement 3.

Domain G, the sutured area between two separate RTT units or crustal plateaus is a unique region in the map area that shows spatial and temporal relationships between separate, and regionally extensive, ribbon tesserae terrains. This suture terrain, or collisional boundary observed in the study area is not addressed in either the mantle downwelling, mantle upwelling, or pulsating continents hypotheses; however, a similar suite of collisional structures termed 'S-C tesserae terrain' is mapped and discussed regarding the lava pond hypothesis (Hansen 2006). The spatial and temporal relationships between structures within the study area coincide with structures predicted in the lava-pond hypothesis, including short-λ folds and ribbon structures trending orthogonal to one another and overlapping in time. If crustal plateaus form from an uplifted lava-pond, and with a high geothermal gradient volcanism still reaches the surface in the areas surrounding the plateaus, the material within the suture zone of the two crustal plateaus would be present and able to deform, causing contractional structures. With crustal

plateaus rising in elevation and continuous volcanism and leaking of lava to the surface across the planet, the crustal plateaus could act as large ‘continents’ moving through a magma ocean. When those ‘continents’ collide, as in domain G, overlying flood material is folded.

6. IMPLICATIONS AND FUTURE WORK

The observed structural relationships between RTT domains C and F and the folded terrain of domain G leads to implications about crustal plateau formation, and illustrates that there is still more information and mapping of crustal plateaus needed to be completed before a general formation hypothesis can be accepted.

The formation of crustal plateaus remains elusive, however with specific questions and further research in appropriate areas, the formation of crustal plateaus can be resolved. This study showed that between two large crustal plateaus there is a zone of folded terrain, possibly forming by collision of the two plateaus. Future research should focus on other crustal plateaus and their margins, to see if collisional zones occur elsewhere. Areas where it is thought that multiple crustal plateaus have formed into one large highland (i.e., Aphrodite Terra) (Fig. 1) provide potentially excellent places to examine the margins of each crustal plateau. Specific problems within this study area still remain, including calculating a quantitative amount of extension within domain B. Further analysis of domain B and the northern part of domain D could provide information regarding the final stage in crustal plateau evolution, and answer whether these areas are related to crustal plateau collapse or some other late deformation.

References Cited

Aubele, J. C. and Slyuta, E. N., 1990. Small domes on Venus: Characteristics and origin. Earth, Moon,, and Planets, v. 50/51, p. 493-532.

Banderdt, B. W., et al., 1997. Plains tectonics on Venus: Venus II Geology, geophysics, atmosphere, and solar wind environment. The University of Arizona Press, Tucson, p. 901-930.

Banks, B. K., 2000. Intratessera Flood-Lava Basins (ITBs) constrain timing of crustal plateau structures, Tellus, Venus [Masters Thesis]: Dedman college, Southern Methodist University.

Banks, B. K. and Hansen, V. L., 2000. Relative timing of crustal plateau magmatism and tectonism at Tellus Regio, Venus. J. of Geophys. Res., v. 105, p. 17,655-17,667.

Barsukov, V. L., et al., 1982. The crust of Venus – Theoretical models of chemical and mineral composition. J. of Geophys. Res., v. 87, p. A3-A9.

Barsukov, V. L., et al., 1986. The geology and geomorphology of the Venus surface as revealed by radar images obtained by Veneras 15 and 16. J. of Geophys. Res., v. 91, p. 378-398.

Basilevsky, A. T., et al., 1986. Styles of tectonic deformations on Venus: Analysis of Venera 15 and 16 data. J. of Geophys. Res., v. 91, p. D399-D411.

Bindschadler, D. L., et al., 1992. Coldspots and Hotspots: Global Tectonics and Mantle Dynamics of Venus. J. of Geophys. Res., v. 97, p. 13,495-13,532.

Davey, S. C. et al., 2013. Hierarchical clustering of pit crater chains on Venus. Can. J. Earth Sci., v. 50, p. 109-126.

DeShon, H. R., et al., 2000. Geologic evolution of southern Rusalka Planitia, Venus. J. of Geophys. Res., v. 105, p. 6983-6995.

Farr, T. G., 1993. Radar Interactions with Geologic surfaces: Guide to Magellan Image Interpretation: JPL Publications 93-24, p. 45-56.

Ford, J. P., 1993. Magellan: The mission and the system: Guide to Magellan Image Interpretation: JPL Publications 93-24, p. 1-5.

Ford, P. G. and Pettengill, G. H., 1992. Venus Topography and Kilometer-Scale Slopes. J. of Geophys. Res., v. 97, p. 13.103-13,114.

Ford, P. G., et al., 1993. Volcanic Features: Guide to Magellan Image Interpretation: JPL Publication 93-24, p. 109-134.
Ghent, R. and Hansen, V. L., 1999. Structural and Kinematic Analysis of Eastern Ovda Regio, Venus: Implications for Crustal Plateau Formation. Icarus, v. 139, p. 116-136.

Gilmore, M. S., 2009. Tellus Regio, Venus: Evidence of Tectonic assembly of tesserae terrain and implications for exploration: Lunar and Planetary Science Conference, 40th Annual Meeting, no. 2015.

Gilmore, M. S. et al., 2010. Mapping and modeling of a tesserae collision zone, Tellus Regio, Venus: Lunar and Planetary Science Conference, 41st Annual Meeting, no. 1769.

Gilmore, M. S. et al., 2011. Constraints on tesserae composition from modeling of Tellus Regio, Venus: Lunar and Planetary Science Conference, 42nd Annual Meeting, no. 2053.

Graupner, M., 2012. Structural and Geologic Mapping of Southern Tellus Regio, Venus: Implications for Crustal Plateau Formation [Masters Thesis]: University of Minnesota Duluth.

Guest, J. E., et al., 1992. Small volcanic edifices and volcanism in the plains of Venus. J. of Geophys. Res., v. 97, p. 15,949-15,966.

Hansen, V. L., 2000. Geologic mapping of tectonic planets. Earth and Planetary Science Letters, v. 176, p. 527-542.

Hansen, V. L., 2005. Venus's shield terrain. Geological Society of America Bulletin, v. 117, n. 808-822.

Hansen, V. L., 2006. Geologic constraints on crustal plateau surface histories, Venus: The lava pond and bolide impact hypotheses. J. of Geophys. Res., v. 111, p. E11010.

Hansen, V. L. and Lopez, I., 2010. Venus records a rich early history. Geology, v. 38, p. 311-314.

Hansen, V. L. and Willis, J. J., 1996. Structural Analysis of a sampling of Tesserae: Implications for Venus Geodynamics. Icarus, v. 123, p. 296-312.

Hansen, V. L. and Willis, J. J., 1998. Ribbon Terrain Formation, Southwestern Fortuna Tessera, Venus: Implications for Lithosphere Evolution. Icarus, v. 132, p. 321-343.

Head, J. W., et al., 1992. Venus Volcanism: Classification of volcanic features and structures, associations, and global distribution from Magellan data. J. of Geophys. Res., v. 97, p. 13,153-13,197.

Kaula, W. M., et al., 1992. Styles of Deformation in Ishtar Terra and Their Implications. J of Geophys. Res., v. 97, p. 16,085-16,120.

Kirk, R. L., et al., 1992. Enhanced visualization for interpretation of Magellan radar data: Supplement to the Magellan Special Issue: J. of Geophys Res., v. 97, p. 16,371-16,380.

McKenzie, D. et al., 1992. Pancakelike Domes on Venus. J. of Geophys. Res., v. 97, p. 15,967-15,976.

Phillips, R. J. and Hansen, V. L., 1994. Tectonic and Magmatic evolution of Venus. Annu. Rev. Earth Planet. Sci., v. 22, p. 597-654.

Phillips, R. J. and Hansen, V. L., 1998. Geological Evolution of Venus: Rises, Plains, Plumes, and Plateaus. Science, v. 279, p. 1492-1497.

Plaut, J. J., 1993. The Non-SAR Experiments: Guide to Magellan Image Interpretation: JPL Publications 93-24, p. 19-31.

Romeo, I. and Turcotte, D. L., 2008. Pulsating continents on Venus: An explanation for crustal plateaus and tesserae terrains. Earth and Planetary Science Letters, v. 276, p. 85-97.

Senske, D. A., 1999. Geology of the Tellus tesserae quadrangle (V10), Venus: Lunar and Planetary Science Conference, 30th Annual Meeting, no. 1668.

Senske, D. A. and Plaut, J. J., 2009. Geologic Evidence for a thick volcanic crust in part of Tellus Tessera, Venus: Lunar and Planetary Conference, 40th Annual Meeting, no. 2015.

Straley, B. L. and Gilmore, M. S., 2007. Mapping and structural analysis of SW Tellus Regio, Venus: Lunar and Planetary Science Conference, 38th Annual Meeting, no. 1657.

Weitz, C. M., 1993. Impact craters: Guide to Magellan Image Interpretation: JPL Publication 93-24, p. 75-92.

Wyrick, D. Y., et al., 2004. Distribution, morphology, and origins of Martian pit crater chains. J. of Geophys. Res., v. 109, p. E06005.

Wyrick, D. Y., et al., 2010. Pit crater chains across the solar system: Lunar and Planetary Conference, 41st Annual Meeting, no. 1413.

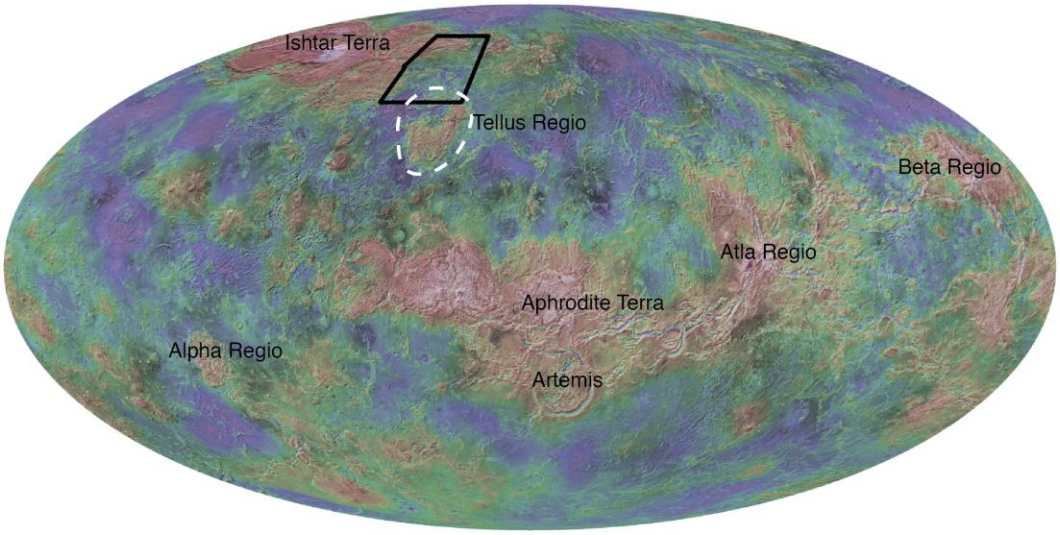

Figure 1. Global altimetry map of Venus showing location of the study area (outlined in solid black) and the commonly defined boundary of Tellus Regio (outlined in dashed white). Highlands are white to red, mesolands are yellow to green, and lowlands are blue to purple.

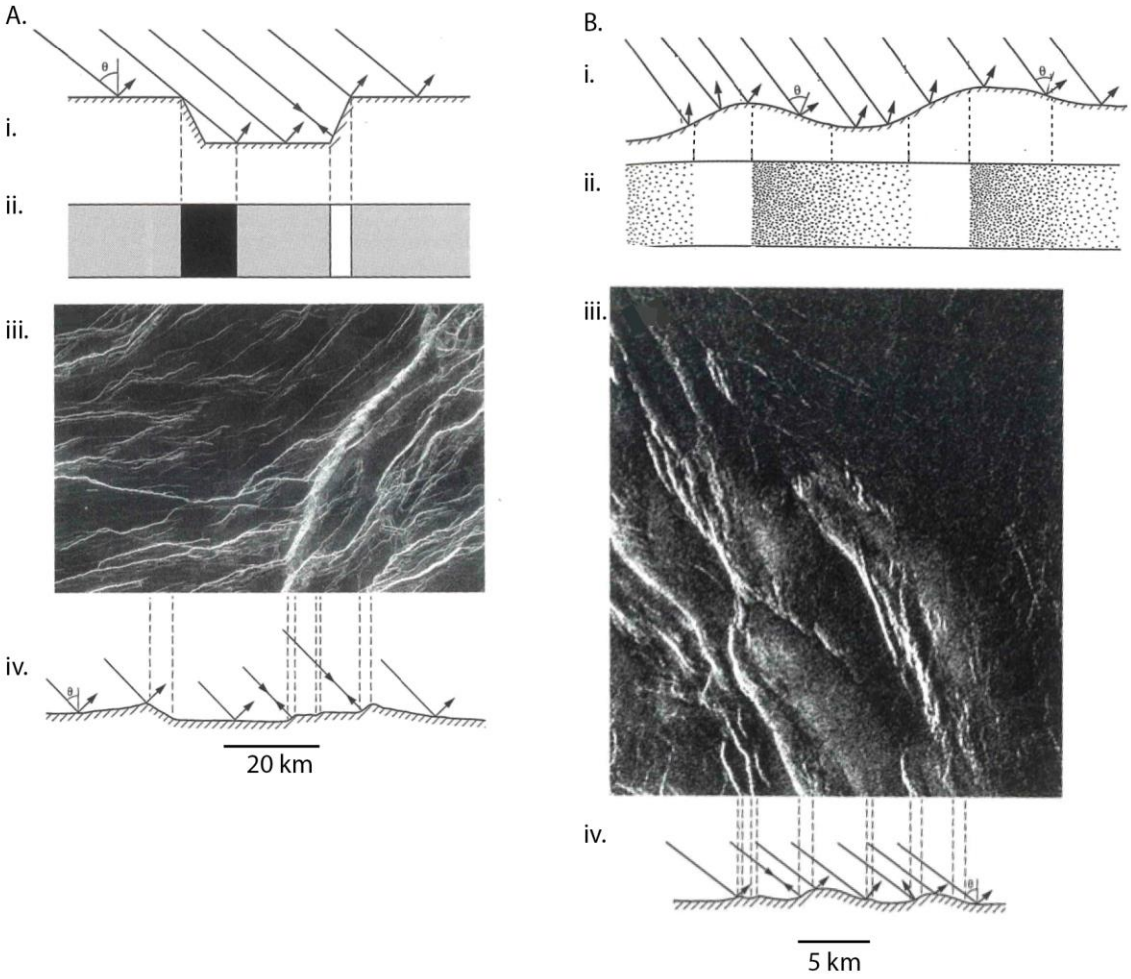

Figure 2. Radar interactions with surface geology for both graben or troughs (A) and folds and ridges (B). Both A and B include a cartoon block diagram (i), the associated radar image (ii), an example SAR image (iii), and the interpreted topography of that SAR image (iv). Radar foreshortening/elongation and radar shadow are shown in A. (Figures modified from Stofan et al. 1993).

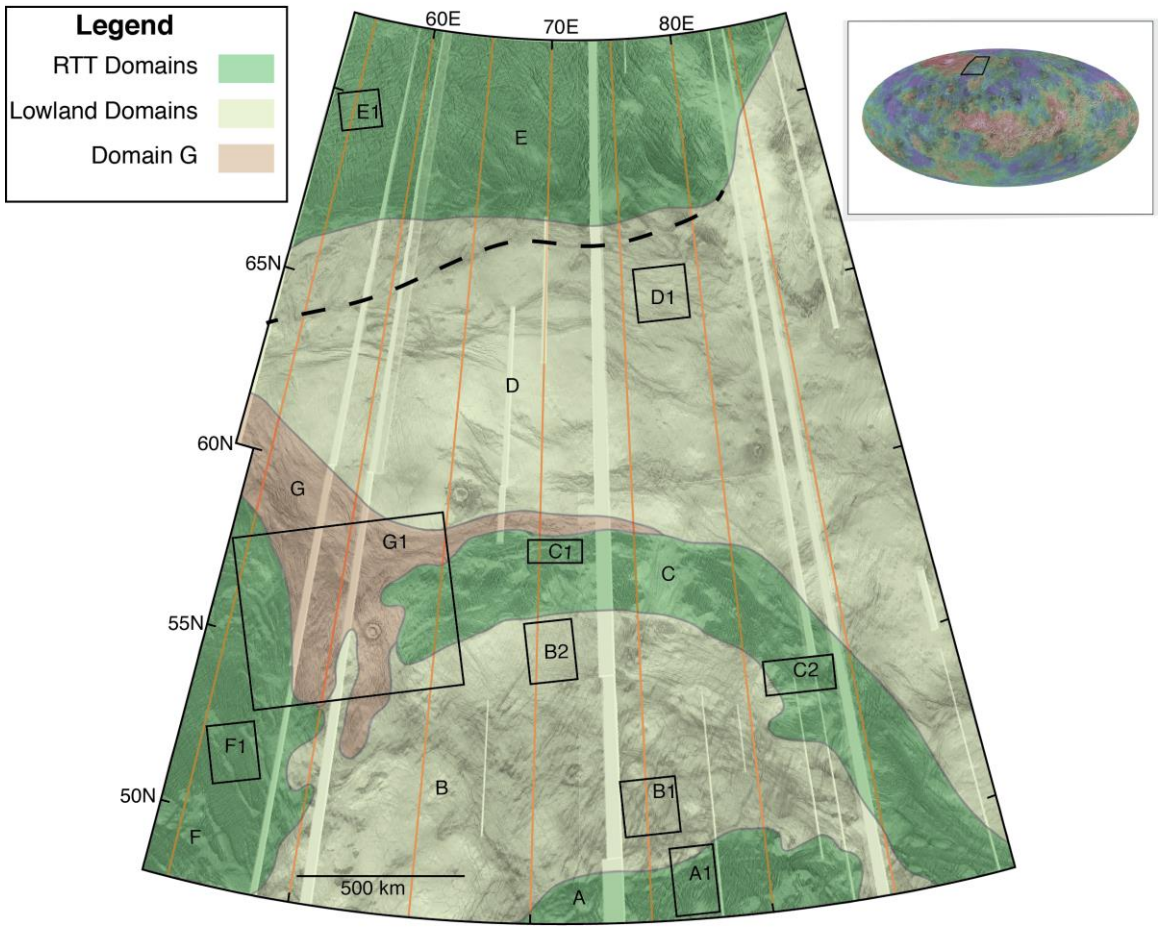

Figure 3. Domain map of northern Tellus Regio, showing the study area divided into domains based on topography and surface roughness. Boxes show locations of targeted mapping areas. Red lines indicate transects for topographic profiles spaced every 5 ° longitude. Black dashed line indicates the southern topographic limit of domain E. Light colored vertical lines are data gaps in the SAR data. The base map, inverted SAR, shows areas of high radar backscatter as dark regions and areas of low radar backscatter as light regions. Inset shows a global surface altimetry map of Venus. Highlands are white to red, mesolands are yellow to green, and lowlands are blue to purple.

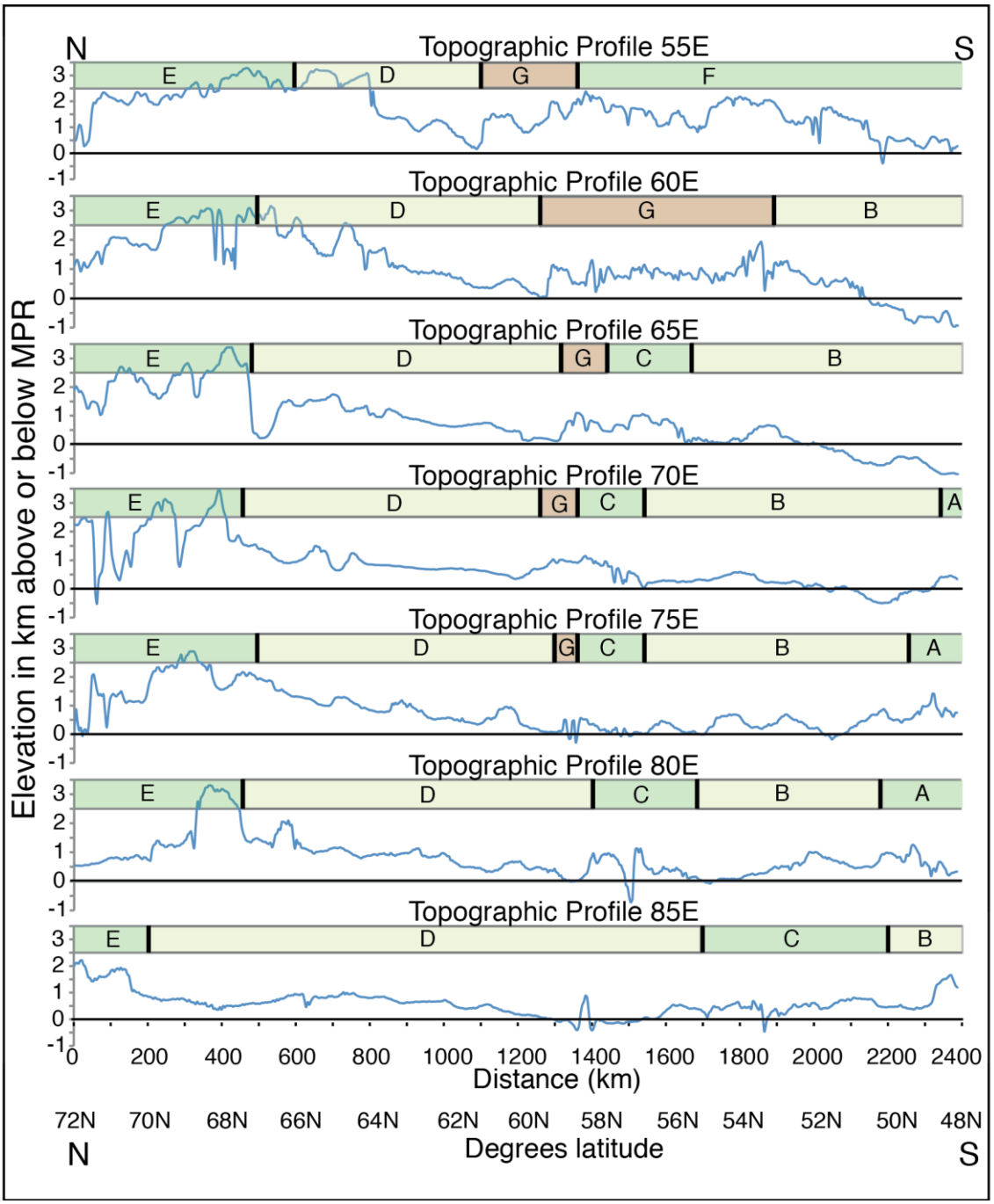

Figure 4. Topographic profiles of seven transects along lines of longitude. Domains are marked with colors; RTT domains are light green, lowland domains are light yellow, and domain G is light brown. The entire study area gradually decreases in elevation from north to south. Mean planetary radius (MPR) is marked by a thicker black line.

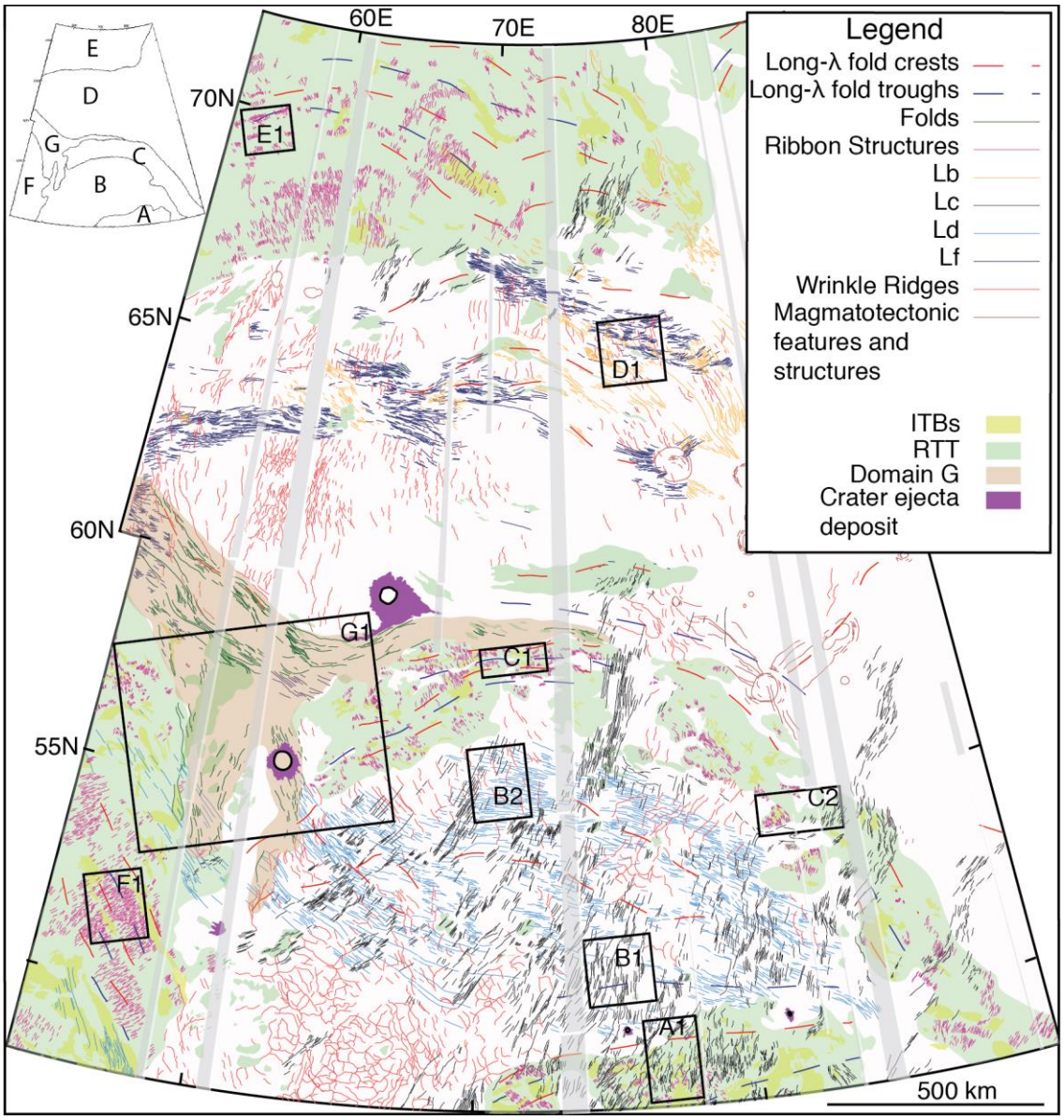

Figure 5. Geologic map of the study area illustrating trends of most structures at a regional scale. Grey lines represent data gaps in the SAR imagery and small boxes represent areas of targeted mapping.

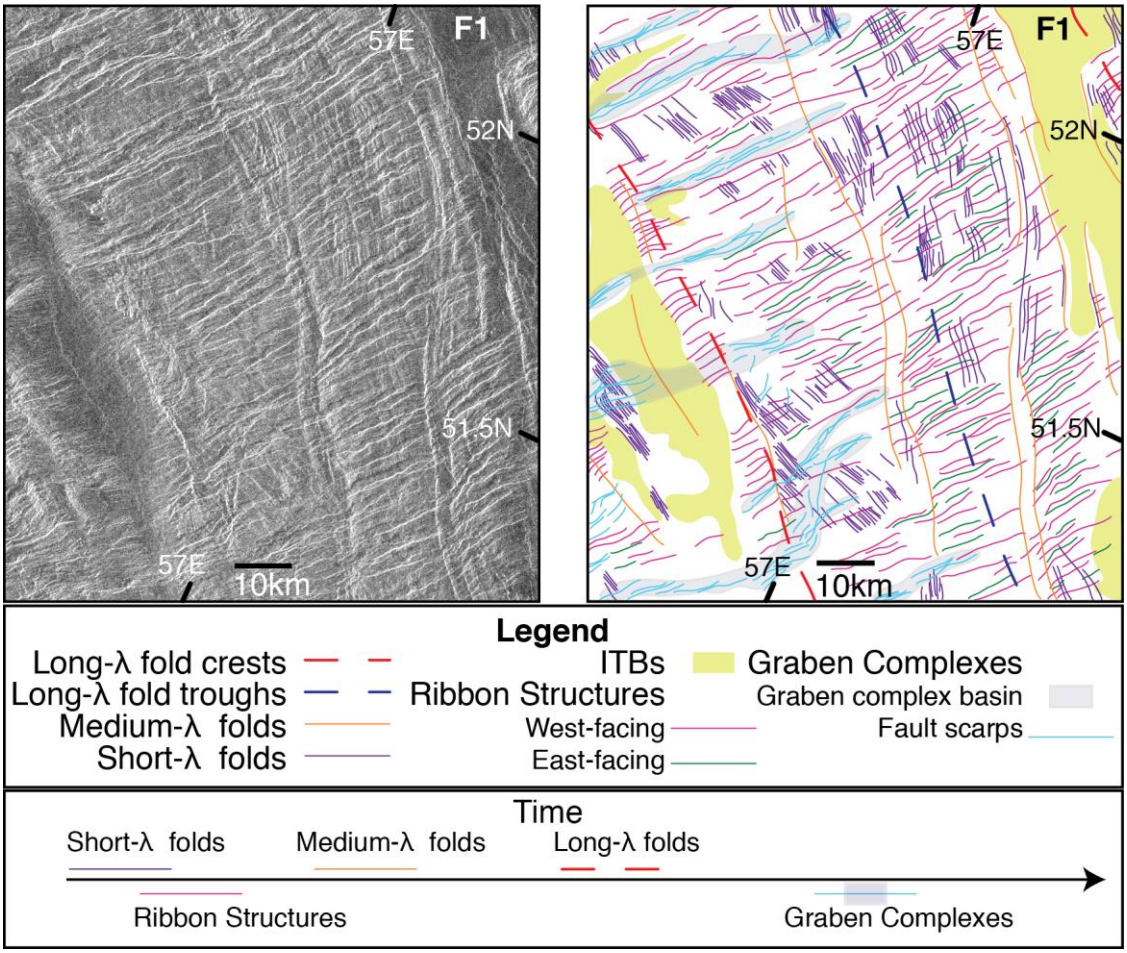

Figure 6. Left-look SAR image, geologic map, and history of target map F1. F1 illustrates an organized, coherent block of RTT fabric. Folds trend NW and ribbon structures and graben complexes trend NE. Temporal relationships between all structures are visible and can be referred to in the text. ITBs occur along the limbs and crests of long-λ folds.

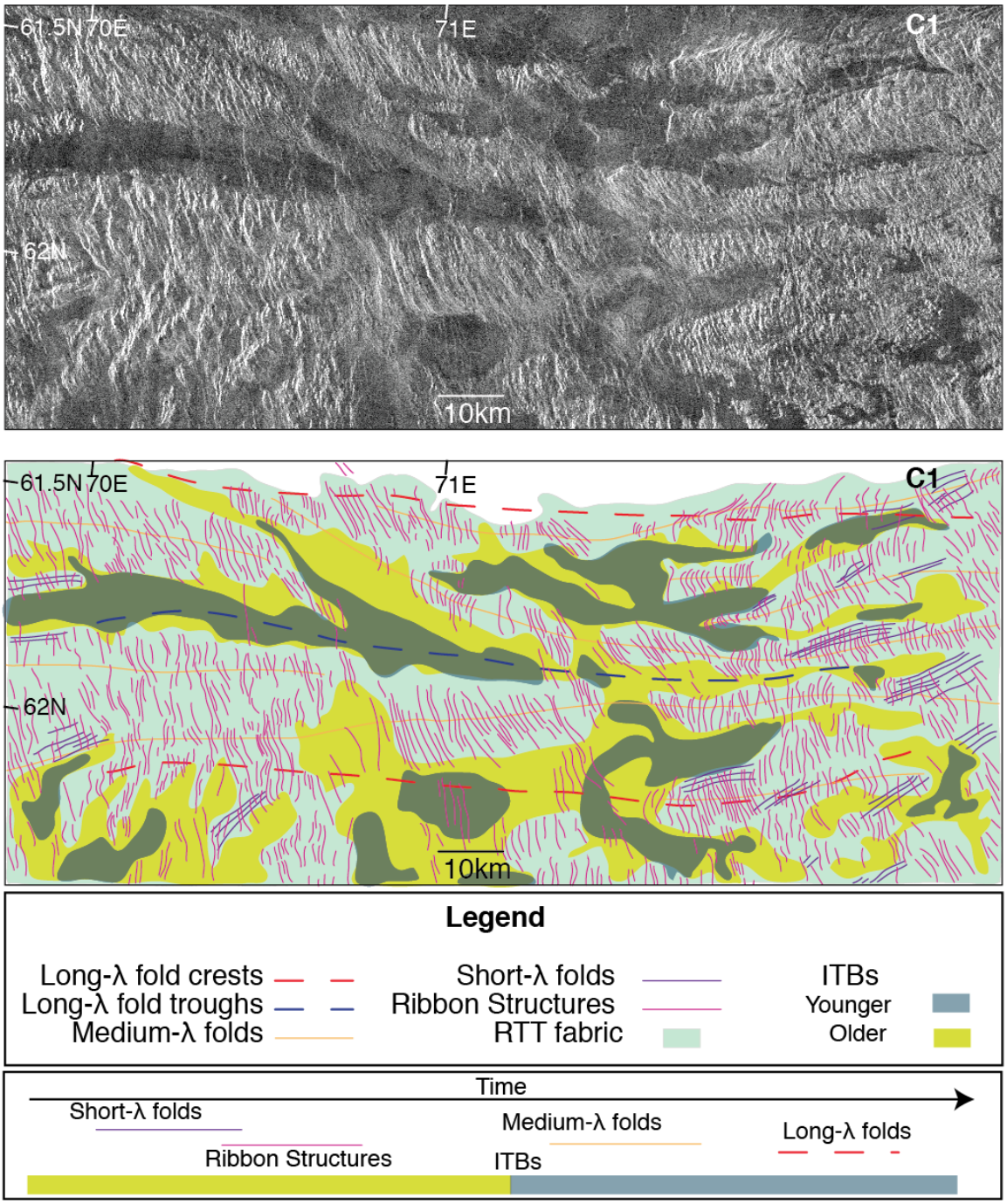

Figure 7. Left-look SAR image, geologic map, and history of target map C1. C1 illustrates the structural trends in domain C and the presence of multiple stages of ITB flooding. The younger ITBs occur along the troughs of medium-λ folds indicating that these ITBs form after medium-λ folds but before long-λ folds.

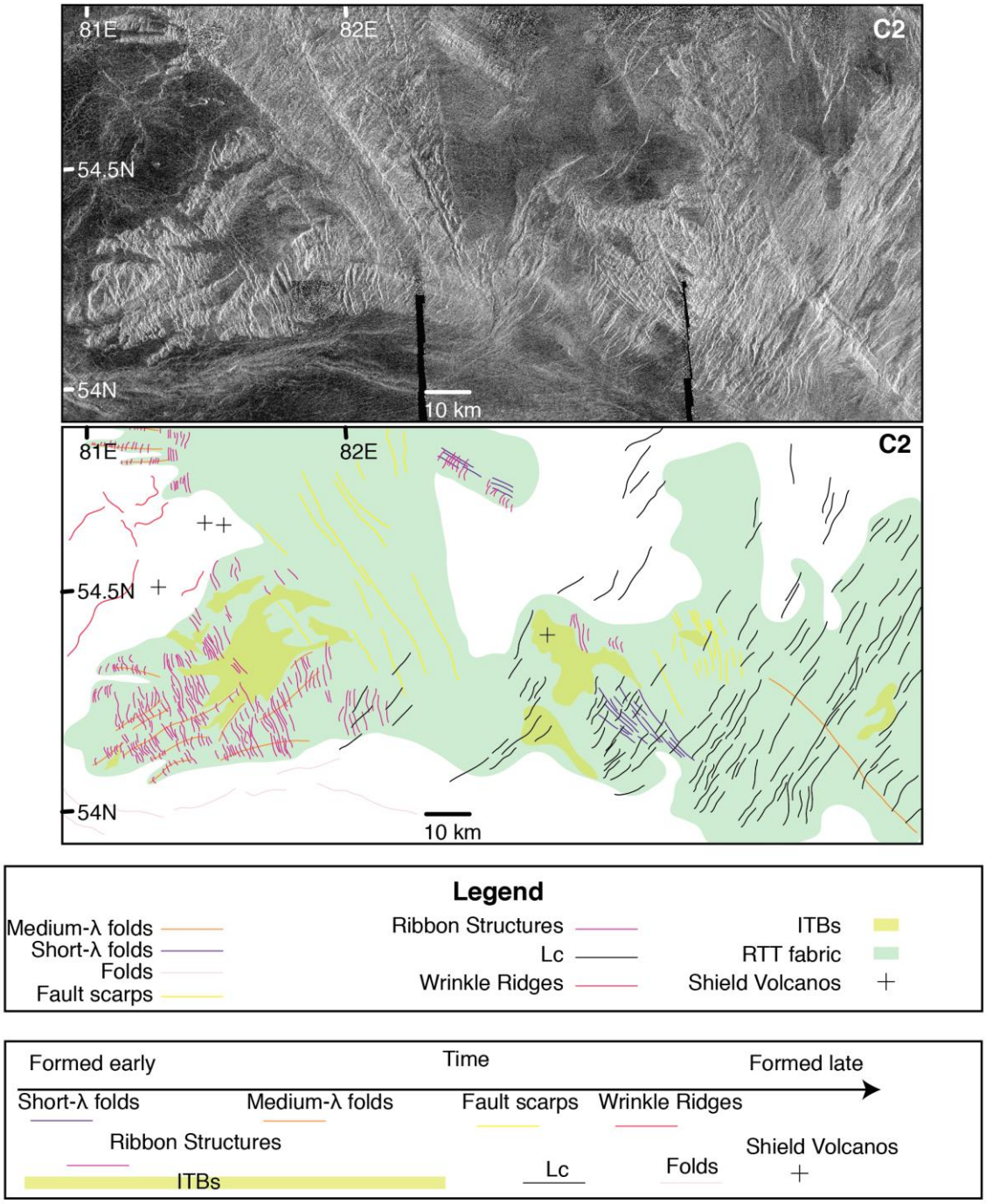

Figure 8. Left-look SAR image, geologic map, and history of target map C2 (Bigfoot). C2 illustrates the presence of long extensional structures with similarities to both ribbon structures and graben. These fault scarps form after RTT formation and trend NW. C2 also illustrates Lc occurring in one of three sections throughout domain C. Lc cut already formed RTT fabric and trend NE.

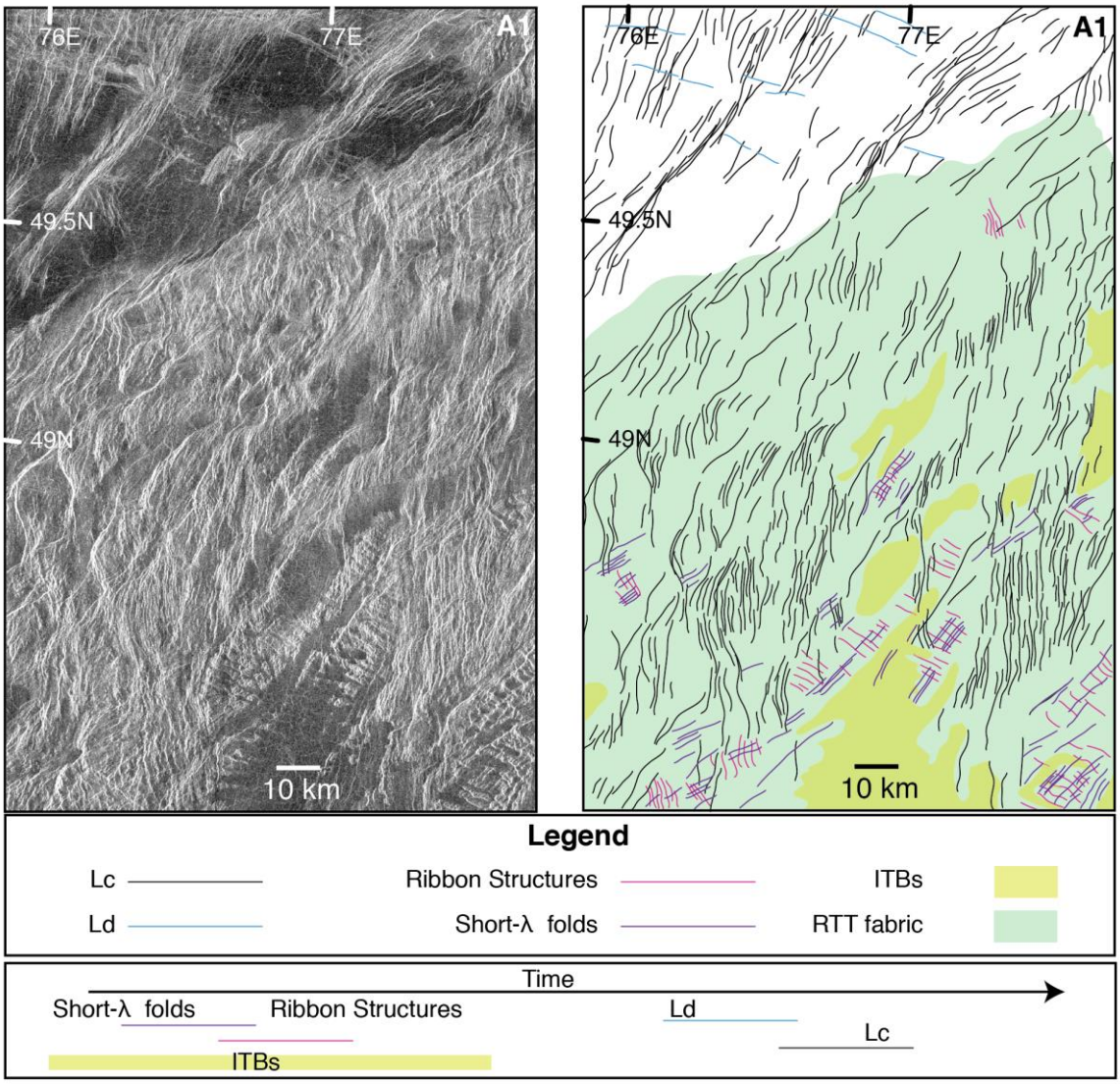

Figure 9. Left-look SAR image, geologic map, and history of target map A1. A1 illustrates Lc cut already formed RTT fabric with ribbon structure trends NW and short-λ fold trends NE.

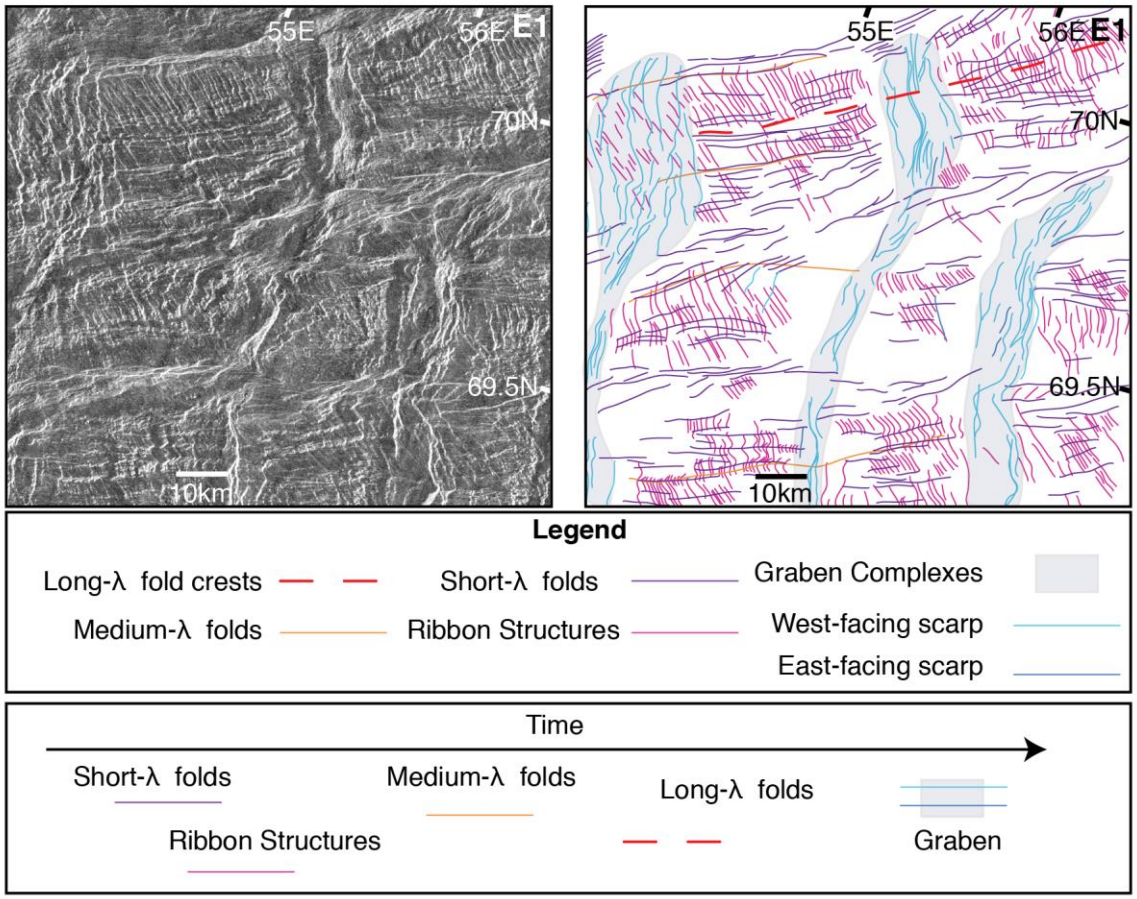

Figure 10. Left-look SAR image, geologic map, and history of target map E1. E1 illustrates graben complexes in RTT fabric displaying a nearly consistent spacing. Graben complexes cut all-λ folds and are the last structures in this map to form. Medium-λ folds cut ribbon structures, which in turn, cut short-λ folds. The ribbon structures in the bottom left corner of the map illustrate radar layover, and display a wriggling character, even though ribbon structures are straight with sharp boundaries between troughs and crests.

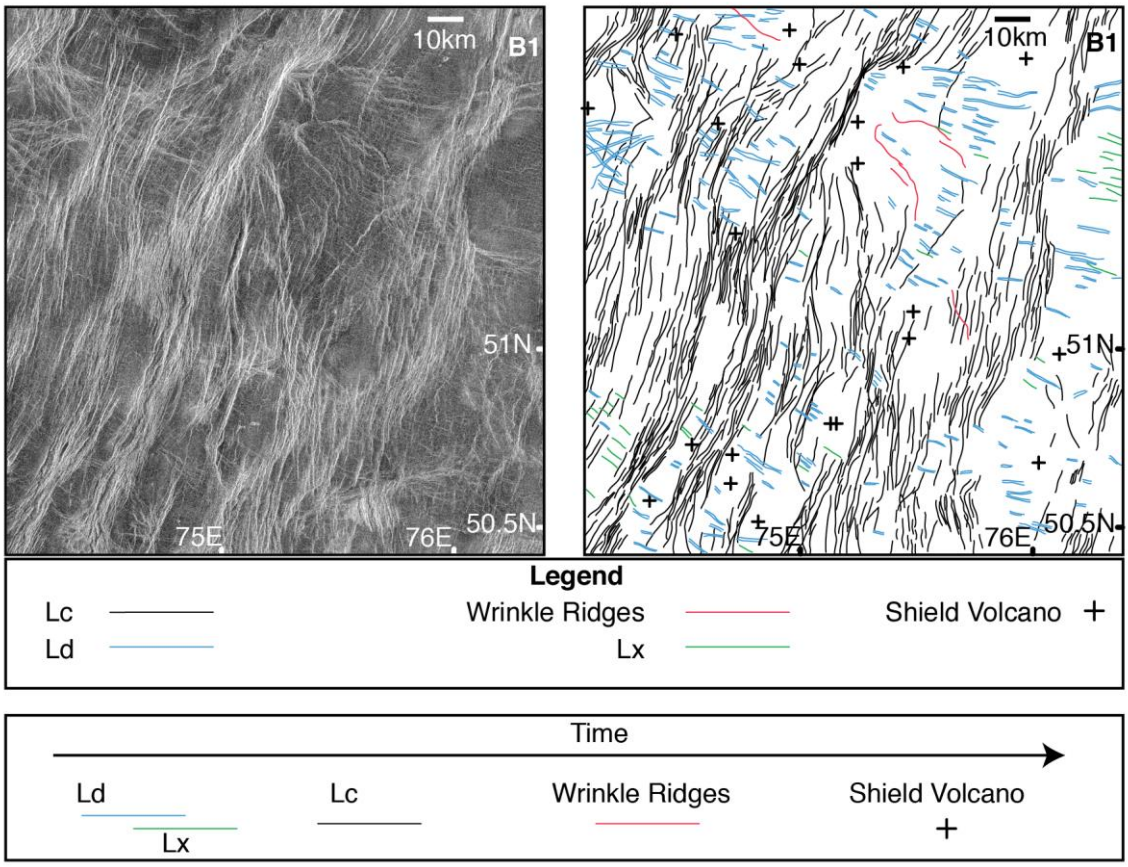

Figure 11. Left-look SAR image, geologic map, and history of target map B1. B1 illustrates the character of Lc and the temporal relations of Lc and Ld.

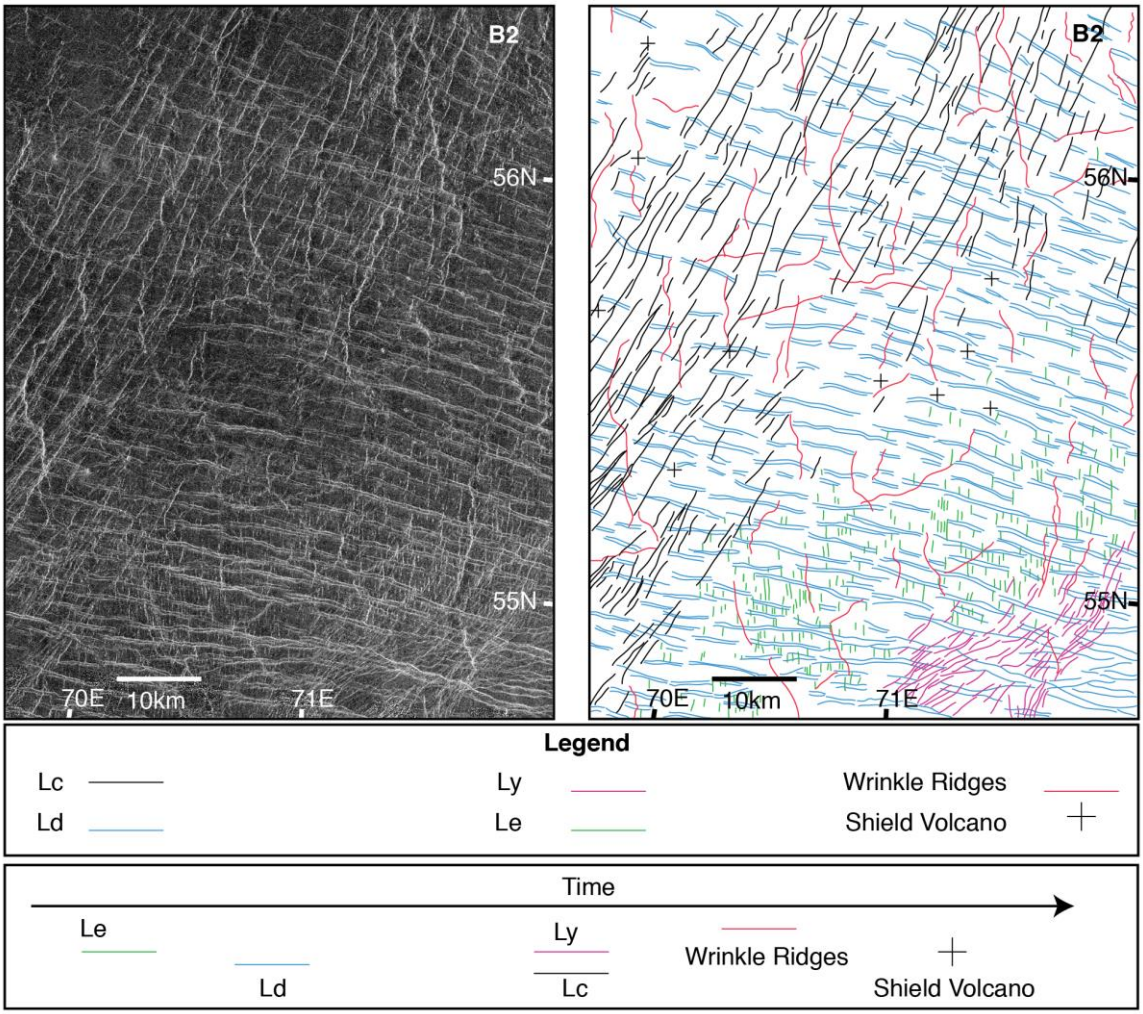

Figure 12. Left-look SAR image, geologic map, and history of target map B2. B2 illustrates the character of Ld and the presence of Le. The temporal relationships between structures are on display and show Lc cut Ld, and wrinkle ridges are the last structure to form.

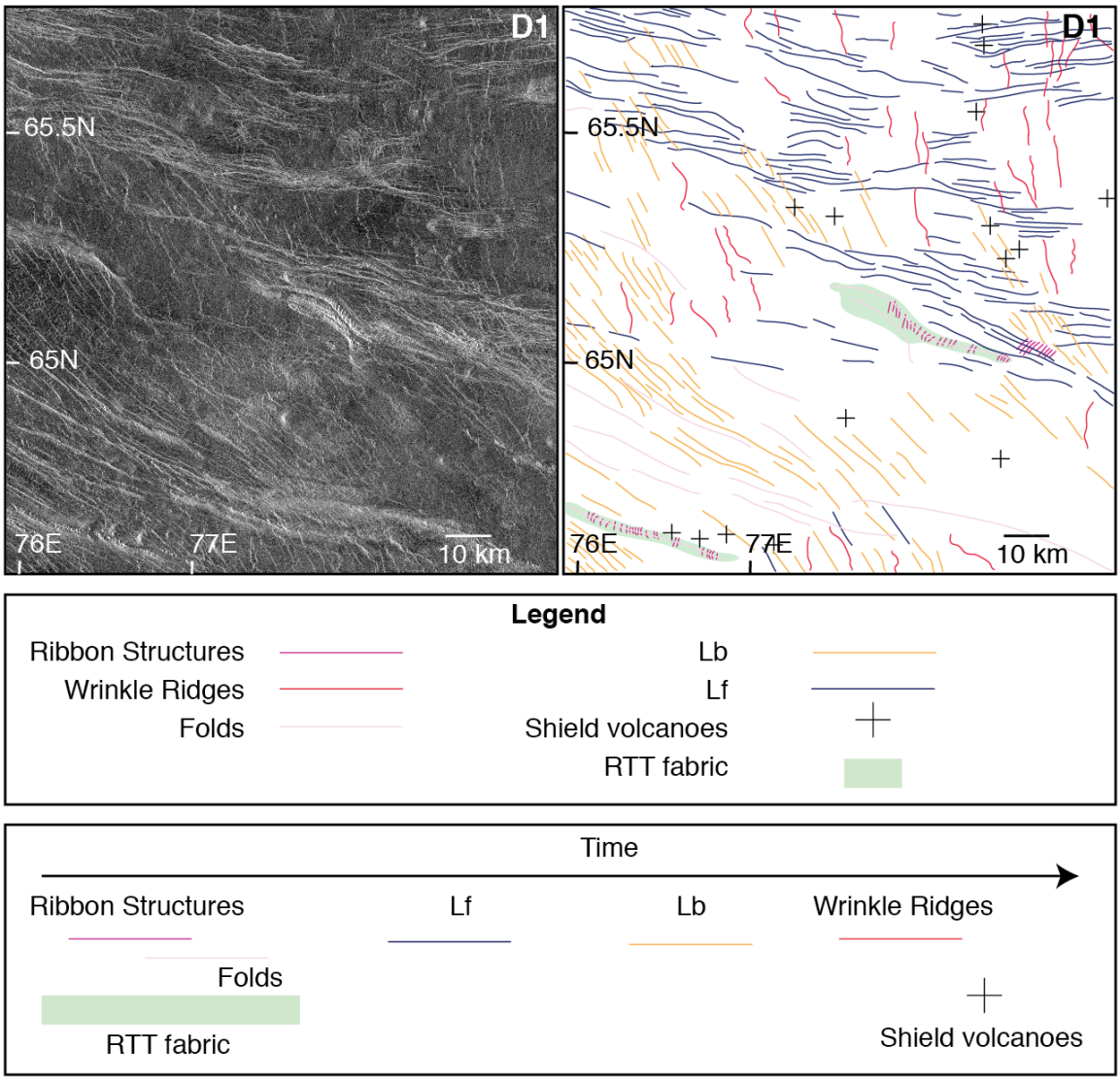

Figure 13. Left-look SAR image, geologic map, and history of target map D1. D1 illustrates relationships between structures in domain D. NW trending Lb cut E-W trending Lf, and both are cut by wrinkle ridges. The RTT kipukas show RTT fabric with folds and ribbon structures. Folds of RTT kipukas trend nearly parallel to Lf and the RTT fabric margin of domain E to the north.

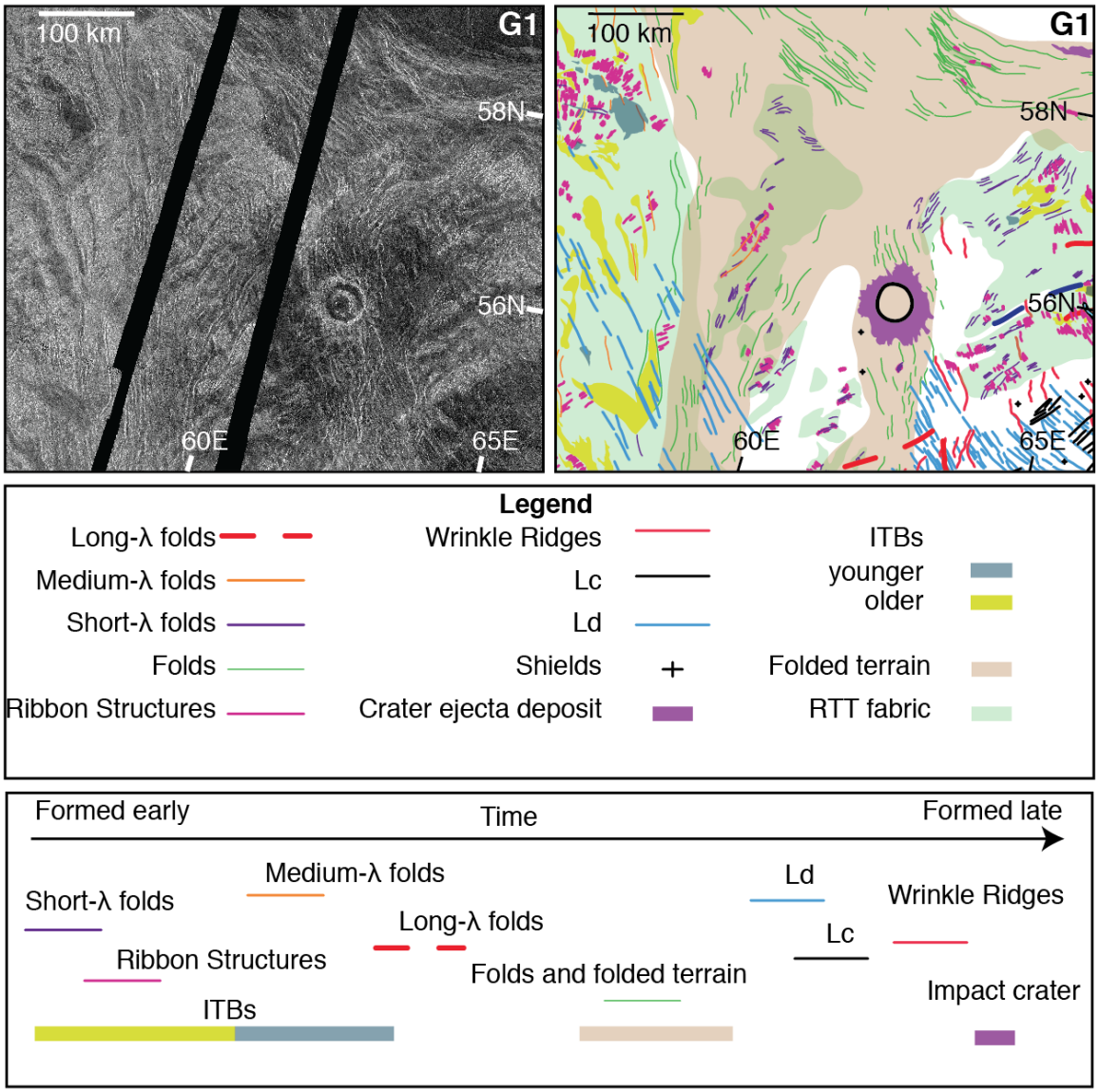

Figure 14. Left-look SAR image, geologic map, and history of target map G1. G1 illustrates the folded terrain associated with the suturing of domains C and F. The RTT structural trends of domains C and F and nearly opposite, and the RTT kipukas within the folded terrain show structural affinity to domain C. The temporal relationships indicate that RTT formed before the folds and suturing of domains C and F. Ld cut the folds and RTT fabric, occurring later, and the last event to occur was the impact, which overprints all structures.

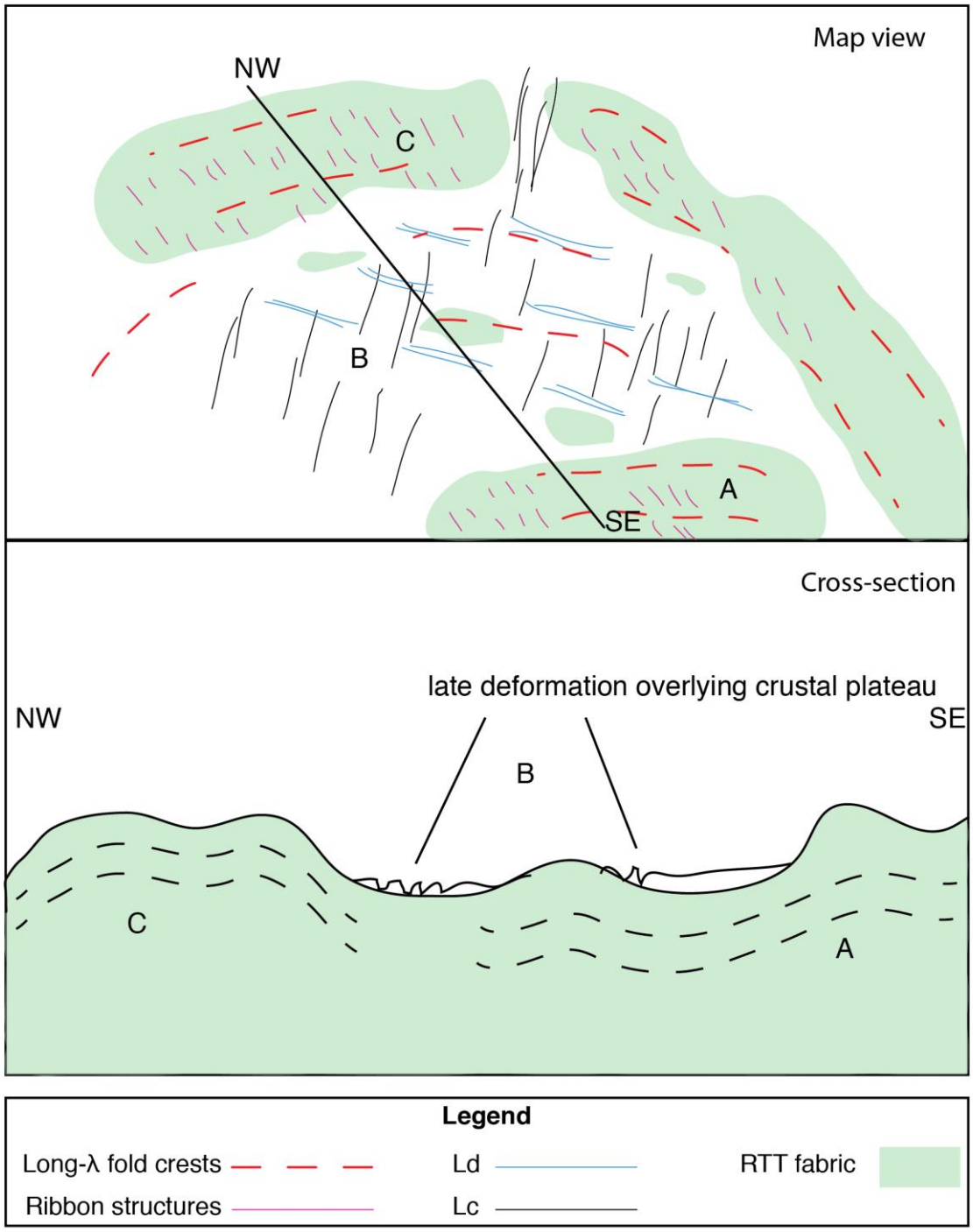

Figure 15. Cartoon diagram showing the cross section of a transect (NW-SE) across domains C, B, and A. The RTT fabric, composing both domains A and C, is present beneath the surface deposits and deformation of domain B. RTT kipukas and long-λ folds occur in areas with a higher elevation than the surrounding terrain. Diagrammatic only with undefined vertical exaggeration.

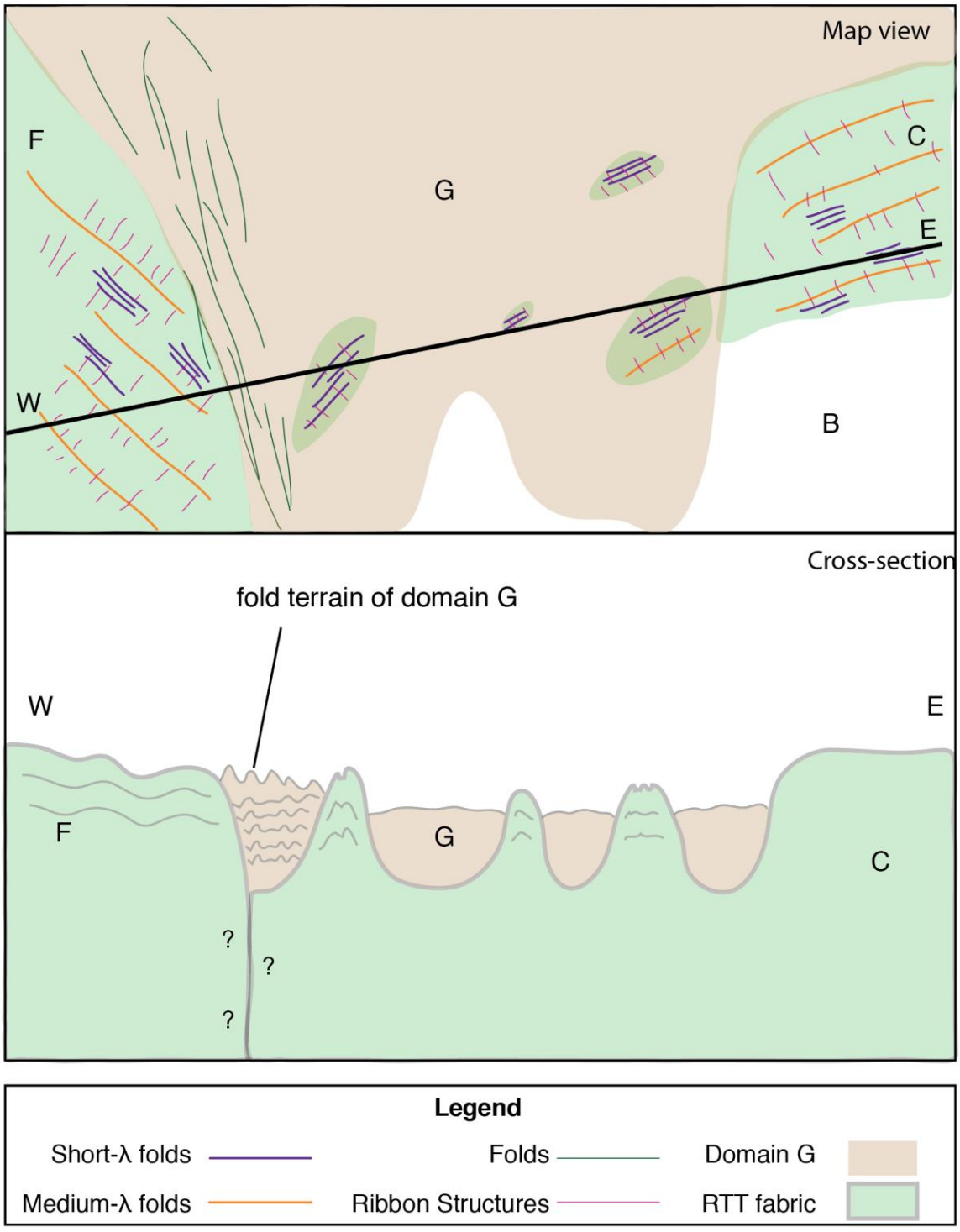

Figure 16. Cartoon diagram showing the cross section of a transect (W-E) across domains F, G, and C. The RTT fabric is present beneath the surface deposits and deformation of domain G. Domains C and F collide and form the folds along the eastern margin of domain F. Kipukas of RTT with structural affinity to domain C, represent areas of domain C with a higher elevation than the surface deposits and deformation in domain G. Diagrammatic only with undefined vertical exaggeration.

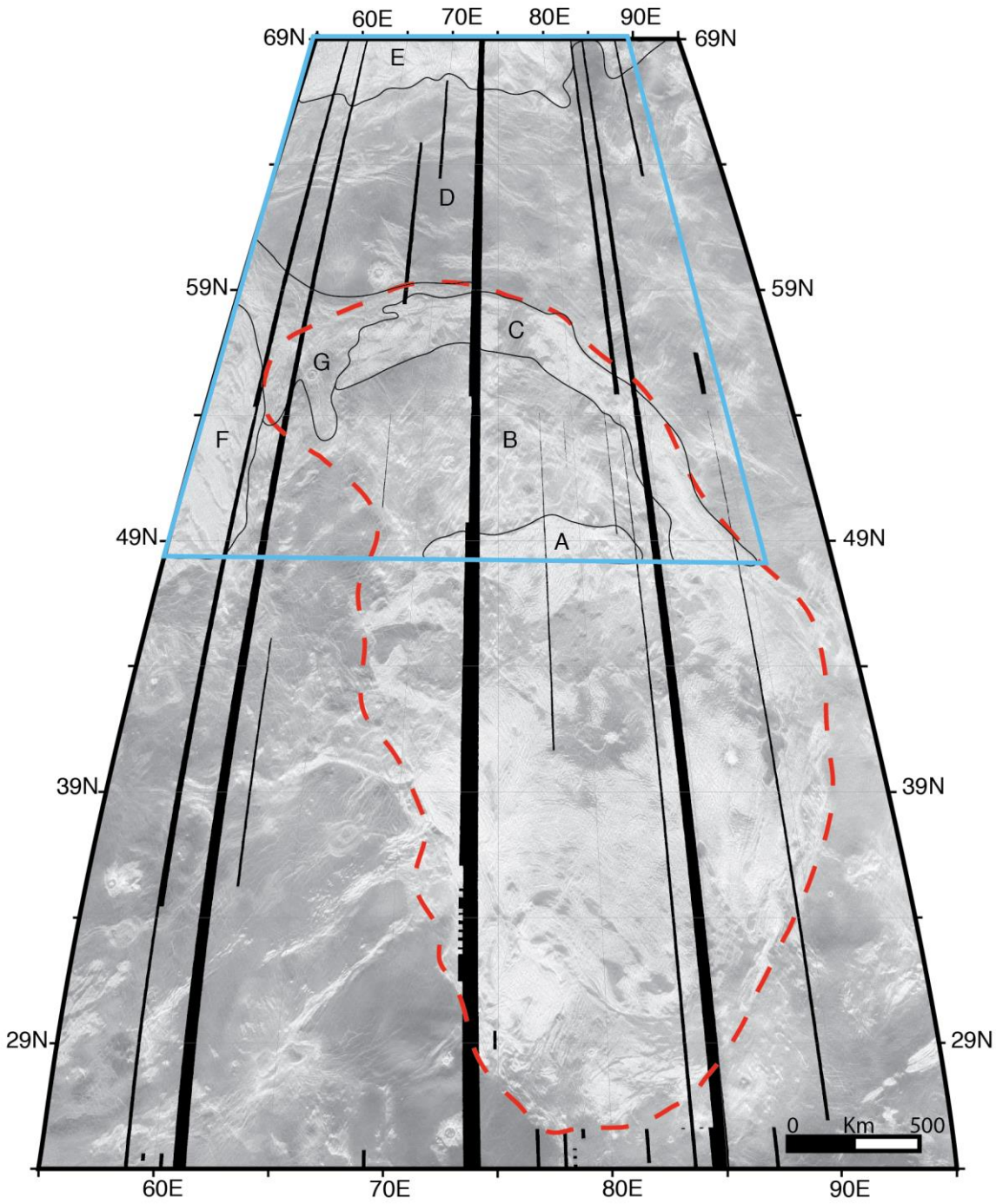

Figure 17. Left-look SAR image of Tellus Regio with the entire crustal plateau outlined in red. The northern boundary of Tellus Regio extends to domain C, and includes domains A, B, C, and G of the study area (outlined in blue).